

Original Article

Selective overexpression of human SIRT1 in adipose tissue enhances energy homeostasis and prevents the deterioration of insulin sensitivity with ageing in mice

Cheng Xu¹, Bo Bai¹, Pengcheng Fan¹, Yu Cai¹, Bosheng Huang¹, Ivy KM Law¹, Ling Liu¹, Aimin Xu¹, Chunling Tung², Xuechen Li², Fung-Ming Siu², Chi-Ming Che², Paul M Vanhoutte¹, Yu Wang¹

¹Department of Pharmacology and Pharmacy, ²Department of Chemistry and Open Laboratory of Chemical Biology of the Institute of Molecular Technology for Drug Discovery and Synthesis, The University of Hong Kong, Hong Kong, China

Received May 6, 2013; Accepted May 21, 2013; Epub May 24, 2013; Published June 1, 2013

Abstract: SIRT1, a longevity regulator and NAD⁺-dependent deacetylase, plays a critical role in promoting metabolic fitness associated with calorie restriction and healthy ageing. Using a tissue-specific transgenic approach, the present study demonstrates that over-expression of human SIRT1 selectively in adipose tissue of mice prevents ageing-induced deterioration of insulin sensitivity and ectopic lipid distribution, reduces whole body fat mass and enhances locomotor activity. During ageing, the water-soluble vitamin biotin is progressively accumulated in adipose tissue. Over-expression of SIRT1 alleviates ageing-associated biotin accumulation and reduces the amount of biotinylated proteins, including acetyl CoA carboxylase, a major reservoir of biotin in adipose tissues. Chronic biotin supplementation increases adipose biotin contents and abolishes adipose SIRT1-mediated beneficial effects on insulin sensitivity, lipid metabolism and locomotor activity. Biochemical, spectrometric and chromatographic analysis revealed that biotin and its metabolites act as competitive inhibitors of SIRT1-mediated deacetylation. In summary, these results demonstrate that adipose SIRT1 is a key player in maintaining systemic energy homeostasis and insulin sensitivity; enhancing its activity solely in adipose tissue can prevent ageing-associated metabolic disorders.

Keywords: SIRT1, NAD⁺-dependent deacetylase, adipose tissue, biotin, longevity regulator

Introduction

SIRT1 (Sirtuin 1) is a member of the NAD⁺-dependent deacetylase family that catalyzes the removal of acetyl groups from protein substrates [1, 2]. Mammalian SIRT1 acts as an energy and stress sensor modulating metabolic responses to nutrient availability. By regulating the acetylation status of different intracellular protein targets, SIRT1 fulfills metabolic functions in an organ- and tissue-specific manner. For example, SIRT1 increases fasting hepatic gluconeogenesis and bile acid homeostasis [3], promotes fat mobilization and adiponectin production from adipocytes [4], enhances insulin secretion in pancreatic β -cells [5], governs the differentiation and regeneration of skeletal muscle fibers [6], and senses nutrient availability in the hypothalamus [7]. Activation of SIRT1 by pharmacological agents protects

mice against diet-induced obesity and insulin resistance, improving the survival and health span of obese mice [8, 9]. Although the available information suggests that SIRT1 is a pharmacological target for the treatment of ageing-associated metabolic disorders, investigations that further determine its tissue-specific actions could justify more targeted therapeutic approaches.

Relative little information is available with respect to the role of SIRT1 in adipose tissue, a pivotal organ controlling lifespan and energy metabolism. In fat-specific Sirt1 knockout mice, systemic and adipose inflammation was observed as early as at four weeks of age [10]. Antisense oligonucleotides-mediated knock down of Sirt1 in both liver and fat stimulates the production of inflammatory factors from white adipose tissue [10]. However, the role of

Sirt1 in glucose or fatty acid metabolism could not be addressed due to anorexia after the antisense treatment [11]. Transgenic mice that have two to three fold increases of Sirt1 expression in most tissues also show adipose tissue inflammation under basal conditions [12]. As Sirt1 is produced by all types of cells, including those of the vascular and inflammatory system, non-specific loss or gain the function of this protein can cause abnormalities of the adipose micro-environment, such as altered blood and oxygen supply [13], which confounds the dissection of its contribution to metabolic regulation.

Mice with specific ablation of Sirt1 expression in their adipocyte-lineage of cells show increased adiposity as early as at one month of age [14]. Both with ageing and under obese conditions, the body weight and adipose tissue contents of these mice were persistently higher than those of the control littermates. In fact, gene expression profiling analysis revealed that the alterations caused by diminished Sirt1 expression in adipose tissue mimics those induced by dietary obesity [14]. However, all results of this study were obtained in female mice, known to be resistant against high fat diet-induced metabolic syndrome [15]. In addition, concerns of the non-specific effects associated with conditional gene targeting based on the Cre/loxP technology have been raised [16].

Sirt1 may be a brown remodeling factor of white adipose tissue [17]. Sirt1-dependent deacetylation of peroxisome proliferator-activated receptor gamma (PPAR γ) contributes to this process. The browning function of Sirt1 is observed in mice that are exposed to mild cold challenge, but not at ambient temperature. Moreover, Sirt1-dependent browning occurs in a heterogeneous fashion and is limited to a specialized subset of adipocytes. Although the above information suggests a beneficial role of SIRT1 in adipose tissue, evidence is lacking from tissue-specific transgenic models, and for supporting its metabolic function during the ageing process.

Two genetically modified mice models that selectively overexpress wild type human SIRT1 (AWSM) or the dominant negative deacetylase mutant SIRT1 (H363Y) (AHSM) in adipose tissues were established. These mice did not exhibit detectable differences (in particular

regarding body weight and fat composition) from wild type littermates at the early stage of life. The metabolic phenotypes only started to diverge after four to five month of age under standard chow conditions, suggesting the suitability of these mice for studying ageing and associated metabolic disorders. Compared to AWSM, AHSM showed a significant deterioration of metabolic performance due not only to the loss-of-deacetylase function of SIRT1 but also other mechanisms, which will be reported separately. In the present study, the characterization was mainly focused on the metabolic phenotypes of AWSM. The results demonstrated that elevation of SIRT1 expression in adipose tissue *per se* prevented the development of ageing-associated insulin resistance, improved systemic energy homeostasis, and enhanced spontaneous locomotor activity. These beneficial effects of SIRT1 can be attributed to the promotion of lipid metabolism in adipose tissue and muscle, resulting in reduced fat accumulation at ectopic sites. The water-soluble vitamin biotin can antagonize the anti-metabolic ageing effects of SIRT1, independently of NAD⁺ bioavailability, in adipose tissue.

Results

Overexpression of human SIRT1 (hSIRT1) in mice adipose tissue prevents the development of ageing-associated metabolic disorders

We generated transgenic mice, which selectively overexpress either wild type hSIRT1 (AWSM) or its dominant negative mutant hSIRT1(H363Y) (AHSM) in adipose tissues. The transgene was driven by adipocyte protein 2 (aP2) promoter [18], and expressed with a Flag tag at the COOH-terminus ([Supplementary Figure 1A](#)). The Flag-tagged hSIRT1 or hSIRT1(H363Y) was detected in epididymal (epi), gluteal (glu), interscapular (inter), perirenal (peri), subcutaneous (sub), and brown (BAT) fats, but not in liver and skeletal muscle ([Supplementary Figure 1B](#) and [1C](#)). Same amounts of tissue extracts were subjected to SIRT1 activity measurement, using an acetylated p53 tri-peptide as the substrate for *in vitro* deacetylation. Compared to wild type mice (WTM), on average, the SIRT1 activity in visceral adipose tissues of AWSM increased 1.7 fold, whereas that of AHSM decreased more than 50% ([Supplementary Figure 1D](#)). The Flag-tagged proteins could be detected in both

SIRT1, adipose tissue and biotin

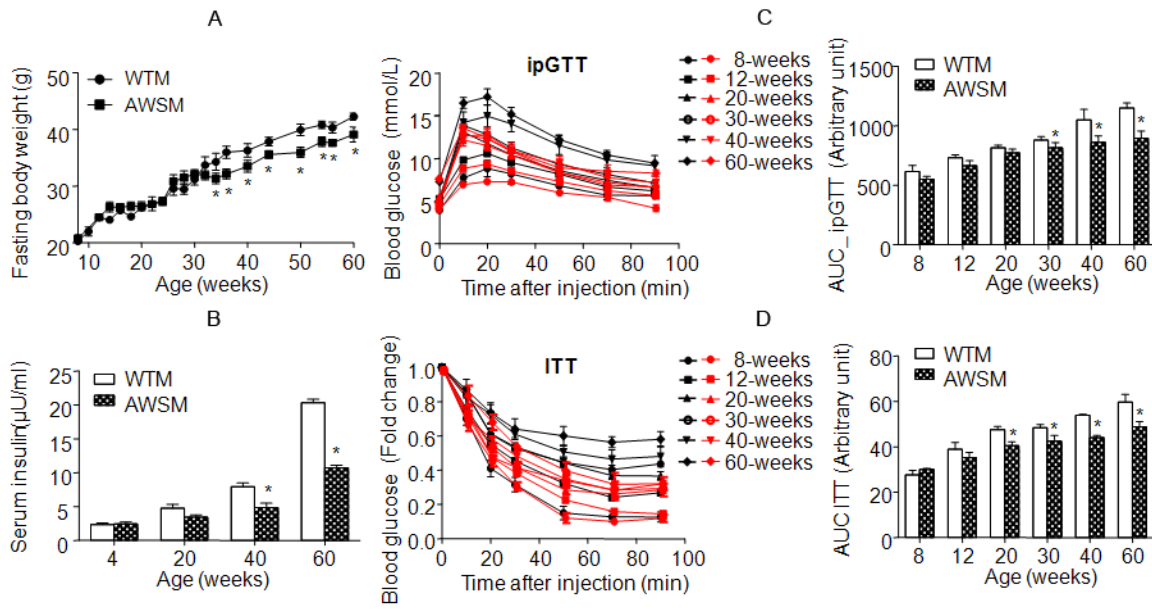


Figure 1. Overexpression of human SIRT1 in adipose tissue of mice attenuates the deterioration of insulin sensitivity with ageing. **A:** Fasting (16 hours) body weights of WTM and AWSM at different ages. **B:** Fasting (16 hours) serum insulin concentrations of WTM and AWSM at different ages. **C:** Intraperitoneal glucose tolerance tests (ipGTT) for WTM and AWSM at different ages. The area under curve (AUC) was calculated and shown in the right panel. Black and red curves represent WTM and AWSM, respectively. **D:** Insulin tolerance tests (ITT) for WTM and AWSM at different ages. The area under curve (AUC) was calculated and shown in the right panel. *, $P < 0.05$ compared with WTM control group ($n=10$).

the adipocytes and stromal vascular fractions isolated from the transgenic animals (Supplementary Figure 2A), an observation in line with findings that aP2 expression marks not only the differentiated adipocytes but also a population of progenitors that reside in the adipose stem cell niche [19]. Increased expression of total SIRT1 protein in adipose tissues of AWSM and AHSM was further confirmed by Western blotting using a polyclonal antibody that recognizes both human and murine SIRT1 (Supplementary Figure 2B). The amount of acetylated histone H4 was significantly decreased in AWSM adipose tissue (Supplementary Figure 2B). The present study mainly focused on the comparison between those of AWSM and WTM.

Mice fed *ad libitum* were monitored until 60 weeks of age. Compared to WTM, AWSM exhibited similar body weight gain, food intake and adipose tissue morphology (data not shown). Fed and fasting blood glucose levels were not different between WTM and AWSM (Supplementary Figure 3). However, from the age of 34-weeks, the fasting body weight of AWSM (16-h food withdrawal with free access

to water) was consistently lower (by 6-10%) than that of WTM (Figure 1A). The age-dependent elevation of plasma insulin levels was significantly attenuated in AWSM (Figure 1B). Compared to age-matched WTM, plasma insulin level was decreased by 39% and 47% in 40- and 60-weeks old AWSM, respectively. In WTM, ageing was associated with a progressive reduction of insulin sensitivity and glucose disposal capacity, as revealed by weekly insulin (ITT) and intraperitoneal glucose (ipGTT) tolerance tests (Figure 1C and 1D). Compared to WTM, the area under curve (AUC) values of ipGTT in AWSM were significantly lower from the age of 30-weeks, whereas the values of ITT AUC in AWSM were significantly decreased from 20-weeks onwards. These results suggest that overexpression of hSIRT1 in mice adipose tissue attenuates the development of ageing-associated insulin resistance.

AWSM show improved fatty acid oxidation capacity and decreased ectopic lipid accumulation

Subsequent metabolic characterization was performed in mice at or older than the age of

SIRT1, adipose tissue and biotin

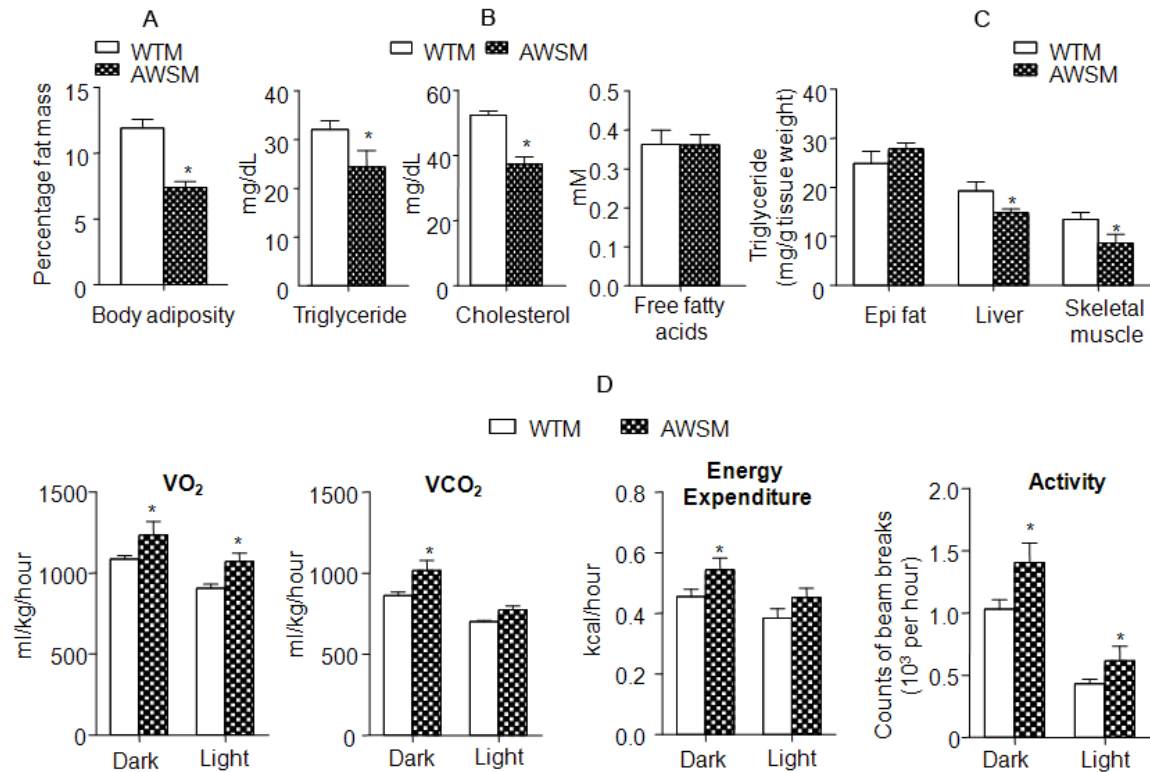


Figure 2. Overexpression of human SIRT1 in adipose tissue of mice improves lipid metabolism, enhances energy expenditure and increases locomotor activity. A: Percentage body fat mass (fat content/body weight%) of WTM and AWSM (36-weeks old, fasted for 16 hours). B: Serum lipid levels of WTM and AWSM (36-weeks old, fasted for 16 hours). C: Lipid measurement in epididymal (epi) fat, liver and skeletal muscle of WTM and AWSM (36-weeks old, fasted for 16 hours). D: Indirect calorimetry analysis of WTM and AWSM (40-weeks old) (light period 0700-1900). *, $P < 0.05$ compared with WTM control group ($n = 10$).

36-weeks. In line with the lower fasting body weights, NMR fat composition analysis revealed that whole body adiposity in AWSM was only ~50% of that in WTM under fasting conditions (**Figure 2A**). The circulating lipid (triglyceride and cholesterol) levels were significantly decreased in AWSM (**Figure 2B**). The wet weights of *post mortem* dissected fat pads and liver tissues were not significantly different between WTM and AWSM (**Supplementary Figure 4A**). However, the triglyceride contents in both liver and skeletal muscle of AWSM were significantly reduced when compared to WTM (**Figure 2C**). Insulin-stimulated glucose uptake was higher in peripheral tissues of AWSM than in those of WTM (**Supplementary Figure 4B**). Energy metabolism was assessed by indirect calorimetry (**Figure 2D**). During the dark cycle, the energy expenditure (EE), oxygen uptake (VO₂) and carbon dioxide output (VCO₂) of AWSM were elevated by ~12-15% when compared to the values of WTM. The respiratory

exchange ratio (RER) of AWSM (0.72 ± 0.021) was significantly lower than that of WTM (0.78 ± 0.016) during the light phase. Moreover, AWSM exhibited elevated locomotor activity, during both the dark and light cycles (**Figure 2D**).

Fatty acid oxidation was evaluated in epididymal fat, liver and skeletal muscle collected from WTM and AWSM. While the fat of AWSM showed only slightly elevated oxidation capacity, fatty acid oxidation rate in soleus muscle of AWSM was significantly increased (more than four-fold) compared to that of WTM (**Figure 3A**). Both circulating and adipose expression of adiponectin [an insulin-sensitizing adipokine [20]] were augmented in AWSM adipose tissue (**Figure 3B**). The mRNA levels of acetyl-CoA carboxylase (ACC) were not different between groups (data not shown); however, the protein expression of ACC was decreased to a barely detectable level in AWSM fat (**Figure 3C**). The

SIRT1, adipose tissue and biotin

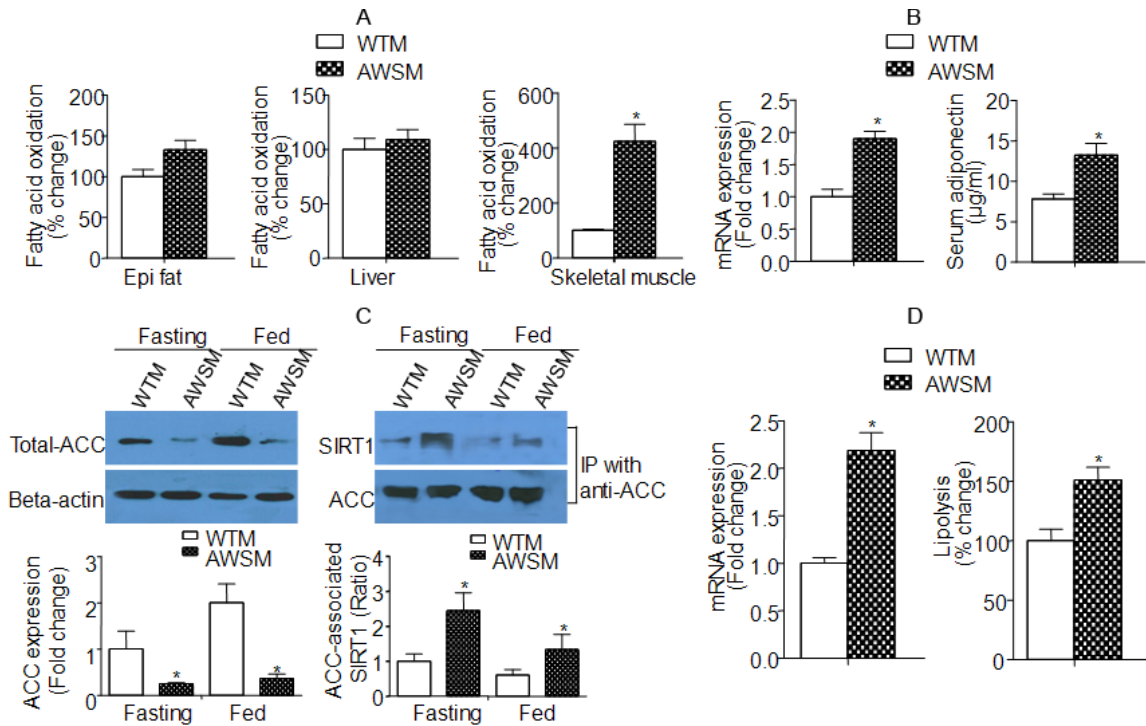


Figure 3. Increased lipolysis and fatty acid oxidation capacity in adipose tissue and skeletal muscle of AWSM, respectively. A: Fatty acid oxidation analyzed using mitochondria extracted from epididymal (epi) fat, liver and skeletal muscle of WTM and AWSM (36-weeks old). B: Left: Quantitative PCR analysis of adipose adiponectin expression; Right: Serum adiponectin levels analyzed by ELISA. C: Left: Western blotting analysis of ACC protein expression in epididymal (epi) fat of WTM and AWSM under fasting and *ad libitum* feeding conditions; Right: Co-immunoprecipitation analysis of the interactions between SIRT1 and ACC. D: Left: Quantitative PCR analysis of adipose ATGL expression; Right: Lipolysis analyzed using epididymal (epi) fat of WTM and AWSM. *, $P < 0.05$ compared with WTM control group (n=3-5).

extremely low levels of ACC protein expression were accompanied by significantly increased interaction between SIRT1 and ACC. Moreover, both acetylated and biotinylated ACC were significantly decreased in AWSM adipose tissue (Supplementary Figure 5). The ACC protein expression in skeletal muscle of AWSM was not different from that of WTM (data not shown). In addition, the expression of adipose triglyceride lipase [ATGL, a rate-limiting lipolytic enzyme [21]] was augmented, in agreement with the increased lipolysis capacity in AWSM adipose tissue (Figure 3D). In skeletal muscle of AWSM, the NAD/NADH ratio was significantly augmented (Supplementary Figure 6).

Taken in conjunction, the above results demonstrate that overexpression of hSIRT1 in adipose tissue *per se* resulted in improved systemic and peripheral tissue lipid metabolism, due in part to a significantly increased fatty acid oxidation in skeletal muscle and lipolysis capacity in adipose tissue.

Chronic biotin supplementation abolishes adipose SIRT1-mediated beneficial metabolic effects

ACC is one of the intracellular protein targets of SIRT1 [22]. It catalyzes the carboxylation of acetyl-CoA to produce malonyl-CoA [an inhibitor of fatty acid oxidation and building block for extending the chain length of fatty acids [23]]. Although ACC protein expression was significantly decreased in adipose tissues of AWSM, the fatty acid oxidation as well as *de novo* lipogenesis (data not shown) were not altered significantly when compared to those in WTM. ACC also represents a major storage reservoir for intracellular biotin, a water-soluble vitamin [24]. A biotinylation site is located within the biotin carboxyl carrier protein (BCCP) domain of the enzyme [25]. Therefore, the global protein biotinylation was compared in adipose tissues of WTM and AWSM. The results revealed that the amount of total biotin and biotinylated proteins was reduced significantly in AWSM fat (Figure

SIRT1, adipose tissue and biotin

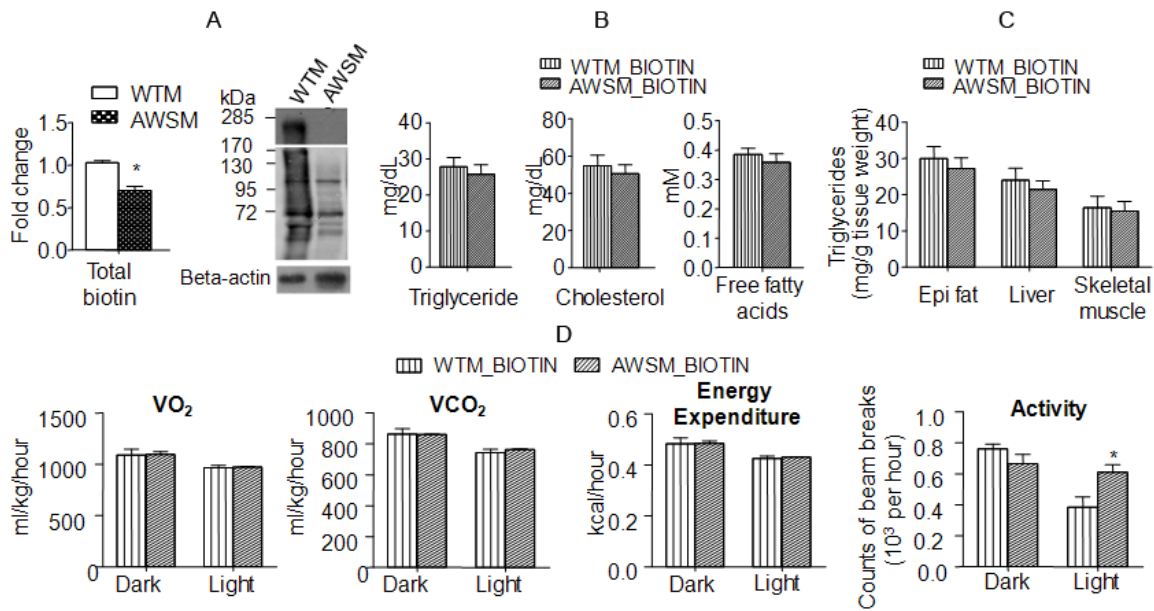


Figure 4. Chronic biotin supplementation abolishes adipose SIRT1-mediated beneficial effects on lipid metabolism and energy expenditure. A: Total (left) and protein-bound (right) biotin in epididymal (epi) fat of WTM and AWSM (36-weeks old) evaluated by ELISA and Western blotting, respectively. B: Serum lipid levels of WTM and AWSM (36-weeks old, fasted for 16 hours). C: Lipid measurement in epididymal (epi) fat, liver and skeletal muscle of WTM and AWSM (36-weeks old, fasted for 16 hours). D: Indirect calorimetry analysis of WTM and AWSM (40-weeks old) (light period 0700-1900). *, $P < 0.05$ compared with the corresponding WTM group ($n = 10$).

4A). In fact, overexpression of hSIRT1 significantly blocked ageing-associated biotin accumulation in adipose tissue, whereas the biotin contents of skeletal muscle and liver tissues were not significantly different between WTM and AWSM (Supplementary Figure 7). On the other hand, the NAD/NADH ratio was not altered in the adipose tissues of AWSM when compared to that in WTM across different age groups (Supplementary Figure 8). In a wild type C57BL/6J mouse (12-weeks old), the biotin contents in adipose tissue (calculated against the same amount of protein) were ~3.5- and ~2.2-fold higher than those in liver and muscle, respectively (Supplementary Figure 9). Thus, considering the wide range of distribution and the large volume (20% of the total body weight in a typical individual) of adipose tissue, it may represent a major biotin reservoir in the body.

To further evaluate whether or not a link exists between intracellular biotin concentration and adipose SIRT1-mediated metabolic function, WTM and AWSM were supplemented with biotin up to the age of 60-weeks. The treatment elevated the biotin contents in adipose tissues of WTM and AWSM to similar levels (59.0 ± 2.20 and 60.2 ± 2.13 nmol/mg protein, respec-

tively), but had no significant effects on those in liver and muscle (data not shown). Glucokinase, a known gene target of biotin [26], was decreased in AWSM fat and elevated by biotin treatment (Supplementary Figure 10). Chronic supplementation with biotin abolished most of the metabolic differences between WTM and AWSM. The responses of WTM and AWSM to ipGTT were similar (Supplementary Figure 11). Circulating lipid levels and skeletal muscle triglyceride contents were comparable between biotin-treated WTM and AWSM (Figure 4B and 4C). Metabolic parameters measured by indirect calorimetry were similar between these two groups of animals, except that the light phase locomotor activity of AWSM remained higher than that of WTM (Figure 4D).

The total protein expression and activity of adipose ACC was not different between the two groups of mice supplemented with biotin (Figure 5A). Immunoprecipitation revealed that the amount of ACC-bound SIRT1 in fat tissues of biotin-treated AWSM decreased to similar levels as those in WTM (Figure 5B). The elevated mRNA expression of ATGL in adipose tissues of AWSM was reduced to a level similar to that in WTM after biotin supplementation (Figure

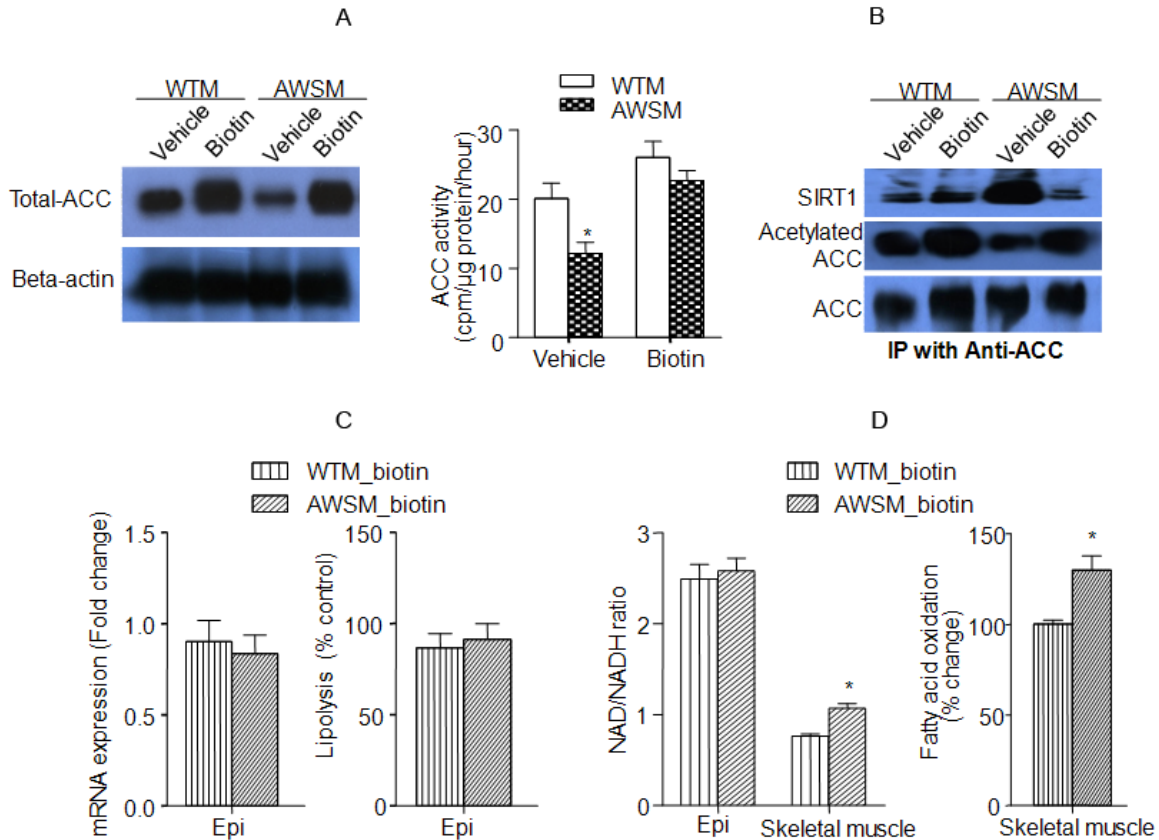


Figure 5. Biotin treatment abolishes hSIRT1-mediated beneficial metabolic effects in adipose tissue and skeletal muscle of AWSM. A: Evaluation of total ACC expression (left) and ACC activity (right) in epididymal fat of vehicle- or biotin-treated WTM and AWSM. B: Co-immunoprecipitation (IP) analysis of SIRT1-ACC interaction and ACC acetylation in epididymal fat of vehicle- or biotin-treated WTM and AWSM. C: Comparison of ATGL mRNA expression (left) and lipolysis rate (right) in epididymal (epi) fat of biotin-treated WTM and AWSM. D: Left: The ratios of NAD/NADH in epididymal (epi) fat and skeletal muscle of biotin-treated WTM and AWSM; Right: Comparison of fatty acid oxidation rate in skeletal muscle of biotin-treated WTM and AWSM. *, $P < 0.05$ compared with corresponding WTM control group (n=5-6).

5C). Consistent with gene expression changes, biotin treatment reduced the lipolysis rate of AWSM fat (**Figure 5C**). The NAD/NADH ratio in skeletal muscles of AWSM remained higher than WTM (**Figure 5D**), although it was decreased significantly in both groups of mice after biotin supplementation (compared to **Supplementary Figure 6**). In addition, the fatty acid oxidation capacity in skeletal muscle of AWSM was significantly decreased by biotin treatment; however, it was still higher than that of WTM (**Figure 5D**).

The above findings suggested that biotin antagonized adipose SIRT1-mediated beneficial effects on energy metabolism and insulin sensitivity. SIRT1 activity was measured in adipose tissue collected from vehicle or biotin-treated AWSM. Chronic biotin supplementation caused

over 50% reduction of SIRT1 activity in AWSM fat (**Supplementary Figure 12A**). The total SIRT1 abundance was not affected by chronic biotin supplementation, whereas the acetylated histone H4 levels in AWSM fat were restored to those observed in WTM fat (**Supplementary Figure 12B**). To further confirm these *in vivo* observations, a vector (pcDNA-BCCP) was constructed for overexpressing the BCCP protein fragment (ACCf) from amino acid 708 to 1053 of human ACC (AAC50139). Transient transfection experiments in 3T3-L1 cells revealed that overexpression of SIRT1 reduced the protein levels of ACCf (**Supplementary Figure 13A**). Biotin blocked the inhibitory effects of SIRT1 on ACCf expression. The SIRT1-ACCf interactions were also inhibited by biotin treatment (**Supplementary Figure 13B**). Moreover, biotin concentration-dependently augmented histone

SIRT1, adipose tissue and biotin

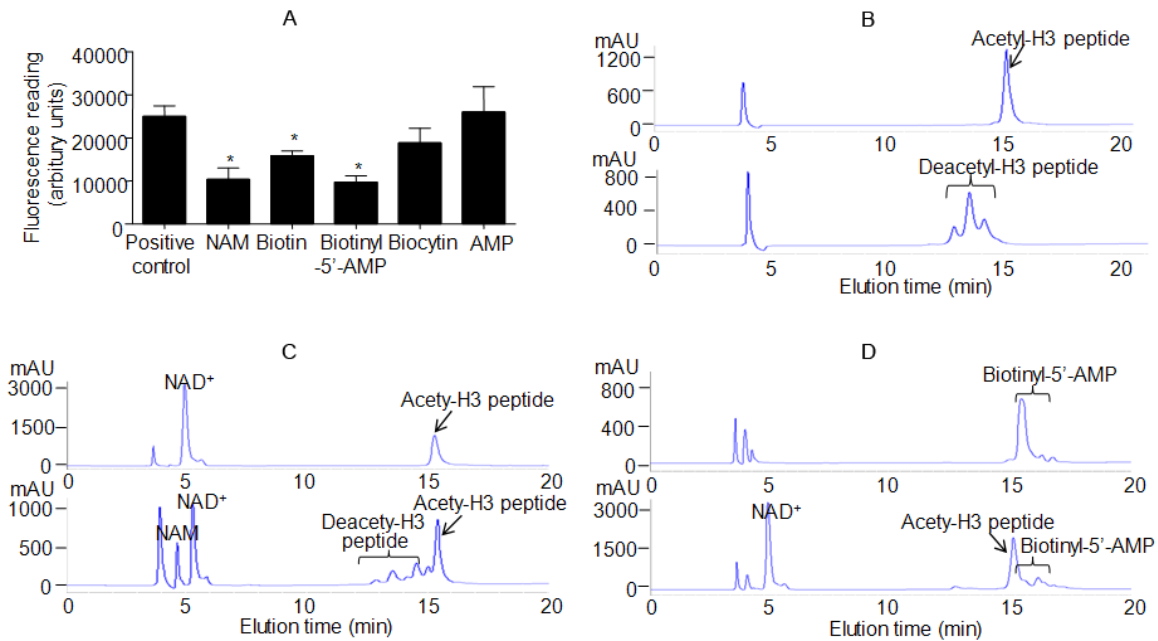


Figure 6. Biotin and biotinyl-5'-AMP inhibit SIRT1-mediated deacetylation reactions. A: *In vitro* deacetylation assay in the absence or presence of 500 μ M nicotinamide (NAM), biotin, biotinyl-5'-AMP, biocytin and AMP. B: HPLC chromatograms of acetylated (top) and deacetylated (bottom) histone H3 peptide. C: HPLC chromatograms of negative (top, reaction without SIRT1 enzyme) and positive (bottom, reaction with SIRT1 enzyme) controls. D: HPLC chromatograms of biotinyl-5'-AMP (top) and positive control reaction in the presence of biotinyl-5'-AMP (bottom). Representative HPLC chromatograms are shown. *, $P < 0.05$ compared with positive control reaction ($n = 8$).

H4 acetylation levels without changing total levels of SIRT1 protein (Supplementary Figure 13C).

Collectively, the above results suggest that biotin may act as a physiological inhibitor of SIRT1 enzymatic activity.

Biotin and its metabolites competitively inhibit the deacetylase function of SIRT1

Biotin exists in both free and protein-bound form. The breakdown product of the latter, biocytin (biotinyl lysine), is cleaved into biotin and lysine. The formation of a biotinyl-5'-AMP intermediate is required for re-conjugating biotin to lysine residues [27]. *In vitro* deacetylation measurements revealed that the addition of 500 μ M biotin or its metabolite, biotinyl-5'-AMP, significantly decreased the fluorescence readings (Figure 6A). The effect of biotinyl-5'-AMP was comparable to that of nicotinamide (NAM), an end product inhibitor of SIRT1 [28]. Biocytin, on the other hand, did not elicit significant inhibition of SIRT1 activity. Subsequently, *in vitro* deacetylation measurements were performed using recombinant human SIRT1 in the pres-

ence of varying amounts of biotin/biotinyl-5'-AMP and NAD⁺. The double reciprocal Lineweaver-Burk plots of the data indicated competitive inhibition of SIRT1 deacetylase activity by both biotin and biotinyl-5'-AMP (Supplementary Figure 14). Biotin was four times less potent ($IC_{50} \sim 200 \mu$ M) than biotinyl-5'-AMP, whereas the latter showed similar potency as that of nicotinamide [28].

Next, high-pressure liquid chromatography (HPLC) was applied to validate the above results. To this end, two peptides (acetylated and deacetylated) derived from the NH₂-terminal tail of histone H3 were synthesized [29, 30]. The purity was checked by HPLC analysis (Figure 6B). Purified recombinant human SIRT1 protein was used for *in vitro* deacetylation using the acetylated H3 peptide. The reaction gave rise to a cluster of peaks that matched exactly the deacetylated peptide standard (Figure 6C). Mass spectrometry confirmed the formation of nicotinamide from NAD⁺ (data not shown). The total amount of NAD⁺ was significantly reduced after the reaction (Figure 6C). When biotinyl-5'-AMP were included, both the nicotinamide and the deacetylated peptide

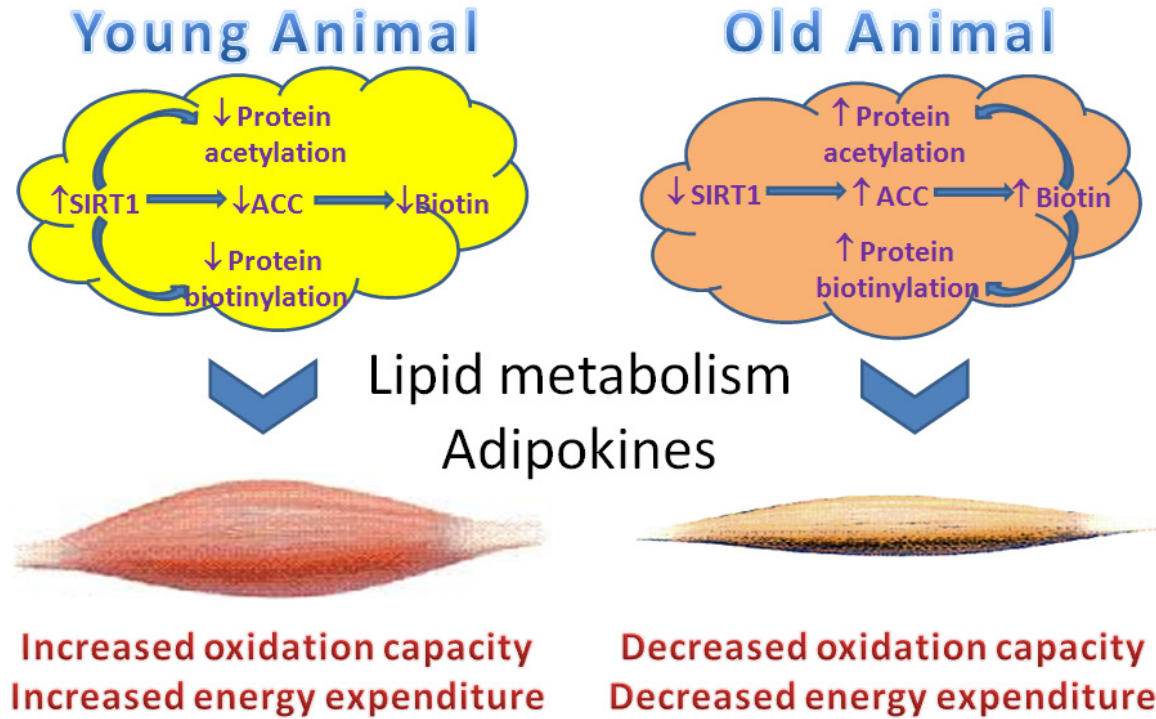


Figure 7. Schematic illustration of SIRT1-mediated regulation of biotin homeostasis in adipose tissues, and the subsequent influence on metabolism in other organs, such as skeletal muscle. During ageing, the regulation balance is lost due to decreased SIRT1 expression and activity, leading to elevated biotin accumulation in adipose tissues, which affects energy metabolisms through both non-genetic (biotin modification of carboxylases) and genetic (biotin modification of histones) mechanisms.

peaks could not be detected in the reaction mixture (**Figure 6D**). Moreover, the amount of NAD^+ was raised to a level similar to that observed in negative control (without SIRT1 enzyme in the reaction mixture, **Figure 6C**).

The concept that biotin and biotinyl-5'-AMP as a physiological inhibitor of SIRT1 was further supported by molecular modeling using the flexible-ligand docking module of ICM-Pro 3.6-1 (Molsoft). SIRT1-catalyzed deacetylation consists of two coupled hydrolysis steps, the cleavage of the glycosidic bond connecting nicotinamide to the ADP-ribose moiety of NAD^+ and the cleavage of the C-N bond between an acetyl group and lysine [31]. A conformational change (non-productive to productive), characterized by relocation of nicotinamide, facilitates the deacetylation of lysine residues [32, 33]. Using the crystal structure of an archeal Sir2 homologue [PDB entry 2H4F [31, 34, 35]], virtual docking demonstrated that biotin occupies the binding site of nicotinamide with a calculated energy of -21.7 kcal/mol (data not shown), whereas biotinyl-5'-AMP, intermediate product

of biotin metabolism, overlapped with NAD^+ with more favorable binding energy (-48.95 kcal/mol) than nicotinamide (-30.2 kcal/mol) (Supplementary Figure 15).

In summary, the above evidence suggests that, by occupying the pockets for nicotinamide and NAD^+ , biotin and biotinyl-5'-AMP can inhibit SIRT1-mediated deacetylation reactions by preventing the binding of acetylated peptide substrates and the consumption of NAD^+ .

Discussion

During ageing, the distribution, composition and function of body fat change dramatically [36]. In advanced old age, while total body fat decreases, the percentage fat composition may increase [37]. Having a proper fat storage in the body helps to postpone organ degeneration (e.g. sarcopenia) and improve the chances of survival in both healthy and unhealthy individuals at older ages [38]. Age-associated decline in adipose depots is accompanied by the accumulation of fat in ectopic organs (such

as liver and muscle), in turn contributing to the deterioration of systemic insulin sensitivity. In fact, interventions that improve adipose function and lipid metabolism can enhance healthy lifespan [39].

Adipose tissue is one of the largest organs in human body and plays a key role in regulating energy metabolism. The present study demonstrates that adipose SIRT1 is critically involved in controlling systemic energy homeostasis. Thus, boosting SIRT1 function selectively in adipose tissue prevents the deterioration of insulin sensitivity with ageing. These effects are largely attributed to improved lipid metabolism (reduced circulating and peripheral tissue lipid content as observed in AWSM). The protein expression of ACC, an enzyme catalyzing the carboxylation of acetyl-CoA to produce malonyl-CoA [the inhibitor of fatty acid oxidation and the building block for extending the chain length of fatty acids [23]], is decreased in adipose tissues of AWSM, which is in line with the enhanced association of this enzyme with SIRT1. By physical interaction, SIRT1 mediates deacetylation and promotes degradation of ACC [22]. Previous studies revealed that ACC in liver and muscle has little effects on systemic energy metabolism, whereas depletion of ACC1 in fat tissue decreases lipid accumulation upon a fat-free lipogenic diet challenge [40]. In the present study, while the total ACC protein levels and activity are decreased, lipid storage is not altered significantly in adipose tissues of AWSM. On the other hand, the mice exhibit an enhanced ability to burn fat in peripheral organs such as skeletal muscle. The fatty acid oxidation capacity in muscles of AWSM is significantly elevated, which largely contributes to their increased locomotor activities and decreased percentage body fat composition.

In addition to its role as an enzyme, ACC is the major storage reservoir for intracellular biotin, a water-soluble vitamin [24]. In mammalian cells, biotin cannot be synthesized *de novo* but is released from biotinylated peptides by biotinidase (EC 3.5.1.12) and recycled for covalent attachment to specific lysine residues by holocarboxylase synthetase (HCS; EC 6.3.4.10). Biotin addition is an ATP-dependent process containing two steps, synthesis of the intermediate, biotinyl-5'-AMP and transfer of biotin, with release of AMP, to lysine residues of protein substrates [41]. In AWSM, ageing-depend-

ent accumulation of biotin in adipose tissue is blocked by hSIRT1 overexpression. Thus, compared to WTM, the amounts of both total biotin and biotinylated proteins are significantly decreased in adipose tissues of AWSM. In mice subjected to long term biotin supplementation, the tissue contents of this vitamin, insulin sensitivity, circulating and tissue lipid concentrations are not different between WTM and AWSM anymore. The ACC expression level in AWSM fat increases, whereas the association of ACC with SIRT1 decreases. Chronic supplementation of biotin inhibits the fat burning capacity in skeletal muscles and the locomotor activity of AWSM. This evidence indicates that the relative biotin deficiency in adipose tissue contributes to the improved metabolic function in AWSM.

Both biotin and biotinyl-5'-AMP inhibits SIRT1-mediated protein deacetylation. Evidence from *in vitro* deacetylation, computer docking and HPLC analysis suggests that biotinyl-5'-AMP competitively occupies the NAD⁺ binding sites and prevents the breakdown of NAD⁺ by SIRT1. Since NAD⁺ also acts as a cofactor permitting SIRT1 to interact with protein substrates [32], by inhibition of NAD⁺ binding, biotinyl-5'-AMP could prevent the interactions between SIRT1 and acetylated protein substrates, such as ACC and histone. On the other hand, biotin occupies the binding pocket of nicotinamide, which may affect the conformational change from non-productive to productive SIRT1 [32, 33]. In addition, biotin may react with NAD⁺ to generate biotinyl-5'-AMP, in turn inhibiting the deacetylase activity of SIRT1. In fact, biotinylated histone peptides are resistant to SIRT1-mediated deacetylation, and acetylated peptides are more likely to be biotinylated than non-acetylated peptides (unpublished observations).

Biotin is a cofactor for carboxylases involved in the metabolism of glucose, amino acids, and fatty acids [42]. Besides its role as a prosthetic group, biotin functions as a gene expression regulator [43]. In adipose tissues of AWSM, significantly increased ATGL expression contributes to the enhanced lipolysis rates. After biotin treatment, ATGL expression in AWSM fat was decreased to WTM levels, along with significantly reduced lipolysis capacity. ATGL plays a key role in the supply of fatty acids to working muscles [44]. Its mRNA levels increase during fasting and decrease during refeeding [45].

Thus, the augmented ATGL expression in adipose tissue of AWSM may facilitate energy supply to contracting muscles and stimulate fatty acid oxidation in peripheral tissues. This explains the unchanged biotin contents in skeletal muscle of AWSM, but the altered NAD/NADH ratios. The mechanism underlying biotin-regulated ATGL expression is not clear. It is not known whether or not biotinylation occurs on forkhead transcription factor, FoxO1. By deacetylating FoxO1, SIRT1 promotes ATGL gene expression [46]. In addition, histones are posttranslationally modified by biotin, which mainly occurs in repeat regions and repressed loci [47]. The biotinyl-5'-AMP intermediate can be conjugated to lysines of histones through a non-enzymatic mechanism [48]. Unlike other modifications (e.g. acetylation and methylation), biotinylation of histone is rare and occurs at a rate less than 0.001% of human histones H3 and H4 [49]. Nevertheless, it is highly possible that histone biotinylation is involved in regulating ATGL gene expressions.

In adipose tissues of AWSM, the expression levels of biotinidase, HCS and sodium-dependent multivitamin transporter are not different from those of WTM (Supplementary Figure 16). The decreased biotin content is mainly due to limited biotin storage and turnover within the cells. Thus, two sets of reciprocal relationships exist between SIRT1 and biotin homeostasis in adipose tissues (Figure 7). In young mice with increased enzymatic function of SIRT1, the amount of ACC is reduced and biotin cannot be efficiently trapped inside adipocytes. Other biotinylated proteins (such as histones) may also contribute to the metabolic trapping and the biotin turnover processes. Limited intracellular supply of biotin will in turn affect carboxylases function, histone modifications, gene transcriptions and chromatin remodeling etc. In old mice with decreased SIRT1 function, the amount of ACC and other biotinylated proteins increases, in turn augmenting the overall storage of biotin and its metabolites in adipose tissues. Biotin, biotinyl-5'-AMP, and biotinylated peptides further suppress the SIRT1-mediated deacetylation of protein substrates. As a result of the above changes, lipid supply from adipose tissues to other organs will be affected. Adipokine (e.g. adiponectin) production will also be affected, in turn contributing to the altered metabolic function in organs such as skeletal muscles (Figure 7).

Taken together, the present study reveals that the intracellular biotin metabolism will have a significant impact on SIRT1 function in adipose tissue, where the biotin storage is abundant and rapidly increasing, but the NAD/NADH ratio remains stable under ageing conditions. In fact, positive associations between biotin concentration and ageing have been observed in humans [50], as well as rodents [51]. In fission yeast, intracellular biotin levels fluctuate according to the nutrient availability: high under excess glucose, diminished with starvation, and virtually absent under growth-arrested fasting conditions [52]. Such changes in biotin concentration may affect Sir2p activity and downstream signaling. In drosophila, biotin affects life span, stress resistance, and fertility [53]. Biotin deficiency for multiple generations increases lifespan and fertility [54]. On the other hand, elevation of SIRT1 expression counteracts biotin accumulation and protein biotinylation in adipose tissue, in turn preventing ageing-induced alterations of metabolism and gene expression. Thus, the reciprocal regulation between SIRT1 function and biotin homeostasis in adipose tissue represents an important therapeutic target for ageing-related metabolic dysfunctions.

Materials and methods (see also in supporting information)

Animal experiments

All procedures were approved by the committee on the use of live animals for teaching and research of the University of Hong Kong and carried out in accordance with the guide for the care and use of laboratory animals. For generating the transgenic mice, a 2.3-kb human SIRT1 (hSIRT1) cDNA fragment from the GST-hSIRT1 construct [22] was sub-cloned into a vector pBS-aP2/pA [55]. The transgenic vector pBS-aP2/hSIRT1 contained the full length hSIRT1 under the control of a 5.4-kb aP2 promoter [56]. Site-directed mutagenesis was performed to generate another transgenic vector pBS-aP2/hSIRT1363dn encoding a dominant negative mutant of human SIRT1, hSIRT1(H363Y), in which the histidine 363 residue was replaced by tyrosine. The transgenic vectors were digested by *NotI* and *BssSI* and an 8.5-kb fragment carrying the aP2 promoter and the transgene was isolated and microinjected into the pronucleus of fertilized eggs of

SIRT1, adipose tissue and biotin

C57BL/6 × CBA mice, as described [18]. Transgenic founders were identified by PCR analysis using two sets of primers (I and II) as listed in [Supplementary Table S1](#). PCR-RFLP was performed using another two sets of primers (III and IV) to verify AWSM and AHSM mice. The transgenic founders were backcrossed with C57BL/6J mice (Jackson Laboratory, Bar Harbor, Maine, USA) for at least 12 generations. The mice were housed in a room under controlled temperature ($23 \pm 1^\circ\text{C}$) and 12-hour light-dark cycles, with free access to water and standard mouse chow (LabDiet 5053; LabDiet, Purina Mills, Richmond, IN). All animals appeared normal and were fertile, giving rise to healthy litters. Male mice were used for this study.

For chronic administration, biotin (Sigma Aldrich, St. Louis, MO, USA) was supplied in the drinking water (10 mg/l). The mean daily water intake was 5 ml/day per mouse. Thus the daily intake of biotin was estimated to be 2.5 mg/kg body weight/day. Mice were assigned randomly to individual experimental groups (n=10 per group). The treatment was started when mice reached the age of eight weeks and continued until the animals were sacrificed at 60 weeks of age. Body weight change and food consumption were monitored on a weekly basis.

Intra-peritoneal glucose tolerance test (ipGTT) and insulin tolerance test (ITT) were performed as described [57]. For ipGTT, overnight fasted mice (16 hours) were given a glucose load by intraperitoneal injection (1 g glucose/kg body weight). For ITT, mice were starved for six hours and then given an intraperitoneal injection of insulin (1 IU/kg body weight). Plasma glucose levels were measured in blood samples obtained from the tail vein at different time points as indicated.

Metabolic parameters

Glucose was measured using an Accu-Check Advantage II Glucometer (Roche Diagnostics, Mannheim, Germany). Triglyceride (TG), total cholesterol (TC), and free fatty acids (FFAs) in serum and tissues were analyzed using LiquiColor® Triglycerides and Stanbio Cholesterol (Stanbio Laboratory, Boerne, TX), and the Half-micro test kit (Roche Diagnostics, Mannheim, Germany), respectively. Fasting serum insulin concentrations were quantified

by the commercial ELISA kits from Mercodia AB (Uppsala, Sweden). Tissue lipid contents, intra-peritoneal glucose tolerance test (ipGTT) and insulin tolerance test (ITT) were evaluated as described [57].

Metabolic analysis by indirect calorimetry

Metabolic rate [V_{O_2} , V_{CO_2} , Respiratory Exchange Ratio (RER) and core body temperature] was measured by indirect calorimetry using a six-chamber open-circuit Oxymax system component of the Comprehensive Lab Animal Monitoring System (CLAMS; Columbus Instruments, Columbus, OH). Mice were maintained at $\sim 23^\circ\text{C}$ under a 12 : 12-h light-dark cycle (light period 0700-1900). Food and water were available *ad libitum*. Animals were housed individually in specially built Plexiglas cages ($5 \times 4.5 \times 8.5$ in.), through which room air was passed at a flow rate of ~ 0.54 l/min. Exhaust air from each chamber was sampled at one-hour intervals for a period of one minute. Sample air was sequentially passed through O_2 and CO_2 sensors for determination of O_2 and CO_2 content. Spontaneous locomotor activity was monitored as photobeam breakage binned every 30 s with a resolution of 10 milliseconds. All mice were acclimatized to the cage for 48 hours before hourly recordings of physiological parameters during a two-days feeding course and a 24 h fasting course. Locomotor activity was binned every 30 s with a 50 ms resolution.

Body composition analysis

Animal body composition was assessed by NMR using a Bruker Minispec Live Mice Analyzer (model mq7.5, LF50, Bruker Optics, Inc) and postmortem dissected weights measurement. NMR is performed in conscious unanesthetized mice. All measurements were performed in duplicate. Indices of percentage fat and lean mass were obtained using this method.

In vitro deacetylation assay

SIRT1 activity was measured with a Fluorometric Drug Discovery kit from Enzo Life Sciences International, Inc (Plymouth Meeting, PA, USA). Fluorescence was measured on a fluorometric reader (Cytofluor II 400 series PerSeptive Biosystems) with excitation set at 360 nm and emission detection set at 460 nm. Reactions

consisted of either 150 ng of recombinant hSIRT1 protein or 20 µg of tissue lysates. For inhibitor assays, reactions were performed in the presence of a range concentrations of NAD⁺ (50, 100, 200, 350, 500 or 700 µM) and either nicotinamide (Sigma), biotin (Sigma), or biotinyl-5'-AMP. Reactions were carried out at 37°C for 20 minutes and analyzed by fluorometry (excitation at 360 nm and emission at 460 nm). Negative controls (without SIRT1 enzyme) were included for normalization.

HPLC analysis

Recombinant human SIRT1 (3.6 µM) was incubated with substrate (acetylated peptide, 500 µM) and NAD⁺ (500 µM) for deacetylation reaction in 50 mM Tris buffer (pH 7.5), in the presence and absence of 500 µM nicotinamide, biotin or biotinyl-AMP. The reaction was carried on at 37°C for 10 min. Trifluoroacetic acid was added to 0.1% before fractionation by HPLC as described [29, 30]. The peptide sequence was ARTKQTARKSTGGKAPPKQLC. The acetyl group was added to the lysine 14 residue to obtain acetylated H3 peptide ARTKQTARKSTGG(AcK)APPKQLC (AcLys14).

Data analysis

All results were derived from at least three sets of experiments. The density of protein bands in Western blotting results were quantitatively analyzed by ImageJ 1.45 software for calculating the expression ratios against loading control. Representative Western blotting images were shown. Statistical calculations were performed with the Statistical Package for the Social Sciences version 11.5 software package (SPSS, Inc., Chicago, IL). The differences in body weights and indirect calorimetry comparison were determined using one-way analysis of variance (ANOVA) with repeated measures. For multiple comparisons, the differences were analyzed by one-way ANOVA, followed by Dunnett's test. Differences in other comparisons were determined by an unpaired two-tailed Student's *t* test. In all cases, statistically significant differences were accepted when *P* was less than 0.05; data are presented as mean ± SEM.

Acknowledgements

This work was supported in part by grants from Seeding Funds for Basic Research of the

University of Hong Kong, Research Grant Council grants (HKU777908M and HKU779712M); the Area of Excellent Scheme (AoE/P-10-01) and the Special Equipment Grant Scheme (SEGHKU02) established under University Grants Committee, HKSAR.

Address correspondence to: Dr. Yu Wang, Department of Pharmacology and Pharmacy, The University of Hong Kong, Hong Kong, China. Tel: (852) 28192864; Fax: (852) 28170859; E-mail: yuwanghk@hku.hk

References

- [1] Wang Y, Xu C, Liang Y and Vanhoutte PM. SIRT1 in metabolic syndrome: where to target matters. *Pharmacol Ther* 2012; 136: 305-318.
- [2] Chalkiadaki A and Guarente L. Sirtuins mediate mammalian metabolic responses to nutrient availability. *Nat Rev Endocrinol* 2012; 8: 287-296.
- [3] Li X. SIRT1 and energy metabolism. *Acta Biochim Biophys Sin (Shanghai)* 2012; 45: 51-60.
- [4] Picard F and Guarente L. Molecular links between aging and adipose tissue. *Int J Obes (Lond)* 2005; 29 Suppl 1: S36-39.
- [5] Bordone L, Motta MC, Picard F, Robinson A, Jhala US, Apfeld J, McDonagh T, Lemieux M, McBurney M, Szilvasi A, Easlson EJ, Lin SJ and Guarente L. Sirt1 regulates insulin secretion by repressing UCP2 in pancreatic beta cells. *PLoS Biol* 2006; 4: e31.
- [6] Tonkin J, Villarroya F, Puri PL and Vinciguerra M. SIRT1 signaling as potential modulator of skeletal muscle diseases. *Curr Opin Pharmacol* 2012; 12: 372-376.
- [7] Coppari R. Metabolic actions of hypothalamic SIRT1. *Trends Endocrinol Metab* 2012; 23: 179-185.
- [8] Baur JA, Ungvari Z, Minor RK, Le Couteur DG and de Cabo R. Are sirtuins viable targets for improving healthspan and lifespan? *Nat Rev Drug Discov* 2012; 11: 443-461.
- [9] Minor RK, Baur JA, Gomes AP, Ward TM, Csiszar A, Mercken EM, Abdelmohsen K, Shin YK, Canto C, Scheibye-Knudsen M, Krawczyk M, Irusta PM, Martin-Montalvo A, Hubbard BP, Zhang Y, Lehrmann E, White AA, Price NL, Swindell WR, Pearson KJ, Becker KG, Bohr VA, Gorospe M, Egan JM, Talan MI, Auwerx J, Westphal CH, Ellis JL, Ungvari Z, Vlasuk GP, Elliott PJ, Sinclair DA and de Cabo R. SIRT1720 improves survival and healthspan of obese mice. *Sci Rep* 2012; 1: 70.
- [10] Gillum MP, Kotas ME, Erion DM, Kursawe R, Chatterjee P, Nead KT, Muise ES, Hsiao JJ,

SIRT1, adipose tissue and biotin

- Frederick DW, Yonemitsu S, Banks AS, Qiang L, Bhanot S, Olefsky JM, Sears DD, Caprio S and Shulman GI. SirT1 regulates adipose tissue inflammation. *Diabetes* 2011; 60: 3235-3245.
- [11] Cho KW and Lumeng CN. SirT1: a guardian at the gates of adipose tissue inflammation. *Diabetes* 2011; 60: 3100-3102.
- [12] Banks AS, Kon N, Knight C, Matsumoto M, Gutierrez-Juarez R, Rossetti L, Gu W and Accili D. SirT1 gain of function increases energy efficiency and prevents diabetes in mice. *Cell Metab* 2008; 8: 333-341.
- [13] Xu F, Burk D, Gao Z, Yin J, Zhang X, Weng J and Ye J. Angiogenic Deficiency and Adipose Tissue Dysfunction Are Associated with Macrophage Malfunction in SIRT1^{-/-} Mice. *Endocrinology* 2012; 153: 1706-1716.
- [14] Chalkiadaki A and Guarente L. High-fat diet triggers inflammation-induced cleavage of SIRT1 in adipose tissue to promote metabolic dysfunction. *Cell Metab* 2012; 16: 180-188.
- [15] Pettersson US, Walden TB, Carlsson PO, Jansson L and Phillipson M. Female mice are protected against high-fat diet induced metabolic syndrome and increase the regulatory T cell population in adipose tissue. *PLoS One* 2012; 7: e46057.
- [16] Qiu L, Rivera-Perez JA and Xu Z. A non-specific effect associated with conditional transgene expression based on Cre-loxP strategy in mice. *PLoS One* 2011; 6: e18778.
- [17] Qiang L, Wang L, Kon N, Zhao W, Lee S, Zhang Y, Rosenbaum M, Zhao Y, Gu W, Farmer SR and Accili D. Brown remodeling of white adipose tissue by SirT1-dependent deacetylation of Pparggamma. *Cell* 2012; 150: 620-632.
- [18] Zhang X, Xu A, Chung SK, Cresser JH, Sweeney G, Wong RL, Lin A and Lam KS. Selective inactivation of c-Jun NH2-terminal kinase in adipose tissue protects against diet-induced obesity and improves insulin sensitivity in both liver and skeletal muscle in mice. *Diabetes* 2011; 60: 486-495.
- [19] Shan T, Liu W and Kuang S. Fatty acid binding protein 4 expression marks a population of adipocyte progenitors in white and brown adipose tissues. *FASEB J* 2013; 27: 277-287.
- [20] Wang Y, Lam KS, Yau MH and Xu A. Post-translational modifications of adiponectin: mechanisms and functional implications. *Biochem J* 2008; 409: 623-633.
- [21] Zimmermann R, Strauss JG, Haemmerle G, Schoiswohl G, Birner-Gruenberger R, Riederer M, Lass A, Neuberger G, Eisenhaber F, Hermetter A and Zechner R. Fat mobilization in adipose tissue is promoted by adipose triglyceride lipase. *Science* 2004; 306: 1383-1386.
- [22] Law IK, Liu L, Xu A, Lam KS, Vanhoutte PM, Che CM, Leung PT and Wang Y. Identification and characterization of proteins interacting with SIRT1 and SIRT3: implications in the anti-aging and metabolic effects of sirtuins. *Proteomics* 2009; 9: 2444-2456.
- [23] Tong L and Harwood HJ Jr. Acetyl-coenzyme A carboxylases: versatile targets for drug discovery. *J Cell Biochem* 2006; 99: 1476-1488.
- [24] Shriver BJ, Roman-Shriver C and Allred JB. Depletion and repletion of biotinyl enzymes in liver of biotin-deficient rats: evidence of a biotin storage system. *J Nutr* 1993; 123: 1140-1149.
- [25] Wakil SJ, Stoops JK and Joshi VC. Fatty acid synthesis and its regulation. *Annu Rev Biochem* 1983; 52: 537-579.
- [26] Chauhan J and Dakshinamurti K. Transcriptional regulation of the glucokinase gene by biotin in starved rats. *J Biol Chem* 1991; 266: 10035-10038.
- [27] Mock DM, Johnson SB and Holman RT. Effects of biotin deficiency on serum fatty acid composition: evidence for abnormalities in humans. *J Nutr* 1988; 118: 342-348.
- [28] Bitterman KJ, Anderson RM, Cohen HY, Latorre-Esteves M and Sinclair DA. Inhibition of silencing and accelerated aging by nicotinamide, a putative negative regulator of yeast sir2 and human SIRT1. *J Biol Chem* 2002; 277: 45099-45107.
- [29] Tanner KG, Landry J, Sternglanz R and Denu JM. Silent information regulator 2 family of NAD-dependent histone/protein deacetylases generates a unique product, 1-O-acetyl-ADP-ribose. *Proc Natl Acad Sci U S A* 2000; 97: 14178-14182.
- [30] Imai S, Armstrong CM, Kaeberlein M and Guarente L. Transcriptional silencing and longevity protein Sir2 is an NAD-dependent histone deacetylase. *Nature* 2000; 403: 795-800.
- [31] Hawse WF, Hoff KG, Fatkins DG, Daines A, Zubkova OV, Schramm VL, Zheng W and Wolberger C. Structural insights into intermediate steps in the Sir2 deacetylation reaction. *Structure* 2008; 16: 1368-1377.
- [32] Min J, Landry J, Sternglanz R and Xu RM. Crystal structure of a SIR2 homolog-NAD complex. *Cell* 2001; 105: 269-279.
- [33] Zhao K, Harshaw R, Chai X and Marmorstein R. Structural basis for nicotinamide cleavage and ADP-ribose transfer by NAD(+)-dependent Sir2 histone/protein deacetylases. *Proc Natl Acad Sci U S A* 2004; 101: 8563-8568.
- [34] Avalos JL, Bever KM and Wolberger C. Mechanism of sirtuin inhibition by nicotinamide: altering the NAD(+) cosubstrate specificity of a Sir2 enzyme. *Mol Cell* 2005; 17: 855-868.
- [35] Hoff KG, Avalos JL, Sens K and Wolberger C. Insights into the sirtuin mechanism from ternary complexes containing NAD+ and acetyl-

SIRT1, adipose tissue and biotin

- lated peptide. *Structure* 2006; 14: 1231-1240.
- [36] Tchkonina T, Morbeck DE, Von Zglinicki T, Van Deursen J, Lustgarten J, Scrbale H, Khosla S, Jensen MD and Kirkland JL. Fat tissue, aging, and cellular senescence. *Aging Cell* 2010; 9: 667-684.
- [37] Hughes VA, Frontera WR, Roubenoff R, Evans WJ and Singh MA. Longitudinal changes in body composition in older men and women: role of body weight change and physical activity. *Am J Clin Nutr* 2002; 76: 473-481.
- [38] Yashin AI, Arbeev KG, Wu D, Arbeeva LS, Kulminski A, Akushevich I, Culminskaya I, Stallard E and Ukraintseva SV. How lifespan associated genes modulate aging changes: lessons from analysis of longitudinal data. *Front Genet* 2013; 4: 3.
- [39] Ahima RS. Connecting obesity, aging and diabetes. *Nat Med* 2009; 15: 996-997.
- [40] Mao J, Yang T, Gu Z, Heird WC, Finegold MJ, Lee B and Wakil SJ. aP2-Cre-mediated inactivation of acetyl-CoA carboxylase 1 causes growth retardation and reduced lipid accumulation in adipose tissues. *Proc Natl Acad Sci U S A* 2009; 106: 17576-17581.
- [41] Chapman-Smith A and Cronan JE Jr. The enzymatic biotinylation of proteins: a post-translational modification of exceptional specificity. *Trends Biochem Sci* 1999; 24: 359-363.
- [42] Roth KS. Biotin in clinical medicine—a review. *Am J Clin Nutr* 1981; 34: 1967-1974.
- [43] Fernandez-Mejia C. Pharmacological effects of biotin. *J Nutr Biochem* 2005; 16: 424-427.
- [44] Schoiswohl G, Schweiger M, Schreiber R, Gorkiewicz G, Preiss-Landl K, Taschler U, Zierler KA, Radner FP, Eichmann TO, Kienesberger PC, Eder S, Lass A, Haemmerle G, Alsted TJ, Kiens B, Hoefler G, Zechner R and Zimmermann R. Adipose triglyceride lipase plays a key role in the supply of the working muscle with fatty acids. *J Lipid Res* 2010; 51: 490-499.
- [45] Zechner R, Kienesberger PC, Haemmerle G, Zimmermann R and Lass A. Adipose triglyceride lipase and the lipolytic catabolism of cellular fat stores. *J Lipid Res* 2009; 50: 3-21.
- [46] Chakrabarti P, English T, Karki S, Qiang L, Tao R, Kim J, Luo Z, Farmer SR and Kandror KV. SIRT1 controls lipolysis in adipocytes via FOXO1-mediated expression of ATGL. *J Lipid Res* 2011; 52: 1693-1701.
- [47] Rios-Avila L, Pestinger V and Zemleni J. K16-biotinylated histone H4 is overrepresented in repeat regions and participates in the repression of transcriptionally competent genes in human Jurkat lymphoid cells. *J Nutr Biochem* 2012; 23: 1559-1564.
- [48] Healy S, Heightman TD, Hohmann L, Schriemer D and Gravel RA. Nonenzymatic biotinylation of histone H2A. *Protein Sci* 2009; 18: 314-328.
- [49] Kuroishi T, Rios-Avila L, Pestinger V, Wijeratne SS and Zemleni J. Biotinylation is a natural, albeit rare, modification of human histones. *Mol Genet Metab* 2011; 104: 537-545.
- [50] Fukuwatari T, Wada H and Shibata K. Age-related alterations of B-group vitamin contents in urine, blood and liver from rats. *J Nutr Sci Vitaminol (Tokyo)* 2008; 54: 357-362.
- [51] Said HM, Horne DW and Mock DM. Effect of aging on intestinal biotin transport in the rat. *Exp Gerontol* 1990; 25: 67-73.
- [52] Pluskal T, Hayashi T, Saitoh S, Fujisawa A and Yanagida M. Specific biomarkers for stochastic division patterns and starvation-induced quiescence under limited glucose levels in fission yeast. *FEBS J* 2011; 278: 1299-1315.
- [53] Landenberger A, Kabil H, Harshman LG and Zemleni J. Biotin deficiency decreases life span and fertility but increases stress resistance in *Drosophila melanogaster*. *J Nutr Biochem* 2004; 15: 591-600.
- [54] Smith EM, Hoi JT, Eissenberg JC, Shoemaker JD, Neckameyer WS, Ilvarsonn AM, Harshman LG, Schlegel VL and Zemleni J. Feeding *Drosophila* a biotin-deficient diet for multiple generations increases stress resistance and lifespan and alters gene expression and histone biotinylation patterns. *J Nutr* 2007; 137: 2006-2012.
- [55] Zhang X, Lam KS, Ye H, Chung SK, Zhou M, Wang Y and Xu A. Adipose tissue-specific inhibition of hypoxia inducible factor 1{alpha} induces obesity and glucose intolerance by impeding energy expenditure in mice. *J Biol Chem* 2010; 285: 32869-32877.
- [56] Ross SR, Graves RA, Greenstein A, Platt KA, Shyu HL, Mellovitz B and Spiegelman BM. A fat-specific enhancer is the primary determinant of gene expression for adipocyte P2 in vivo. *Proc Natl Acad Sci U S A* 1990; 87: 9590-9594.
- [57] Law IK, Xu A, Lam KS, Berger T, Mak TW, Vanhoutte PM, Liu JT, Sweeney G, Zhou M, Yang B and Wang Y. Lipocalin-2 deficiency attenuates insulin resistance associated with aging and obesity. *Diabetes* 2010; 59: 872-882.

Supporting Information

Materials and Methods

Glucose and fatty acid uptake, lipogenesis, lipolysis and fatty acid oxidation. Glucose uptake was determined in isolated fat pads or skeletal muscle strips as described [1]. For measuring fatty acid uptake, epididymal adipose tissue or soleus muscle was incubated in preoxygenated buffer (120 mM NaCl, 4.8 mM KCl, 1.2 mM MgSO₄, 25 mM NaHCO₃, 1.2 mM NaH₂PO₄, 1.3 mM CaCl₂, pH7.4) for 30 minutes at 37°C. This was followed by another 30 minutes of incubation in fresh buffer with or without 100 nM insulin. Fatty acid uptake was initiated by adding 20 μM palmitic acid and 0.5 μCi/ml ³H-palmitic acid. The reaction was stopped after five minutes. Non-specific uptake was measured in the presence of excess amount of palmitate (2 mM) and subtracted from all other values. The tissues were dissolved in 1M NaOH and neutralized with 1M HCl.

For assaying lipogenesis, adipose tissue was incubated in preoxygenated buffer containing 5.5 mM glucose in the presence of [U-¹⁴C]glucose (1 μCi/ml) or ³H₂O (1 μCi/ml). After two hours of incubation, total lipids were extracted from the tissues by chloroform/methanol method as described [1]. The radioactivity was determined by scintillation counting and results normalized against the total protein amount.

For lipolysis analysis, the epididymal fat pad was incubated in oxygenated Krebs-Ringer solution (120 mM NaCl, 4.8 mM KCl, 1.3 mM CaCl₂, 1.2 mM MgSO₄, 1.2 mM KH₂PO₄, 25 mM NaHCO₃, 6 mM glucose and 0.1 mM ascorbic acid, pH 7.6) at 37°C for 60 minutes in sealed plastic vials oscillating at 50 times/min. The amount of glycerol released into the media was measured with a colorimetric assay kit from Cayman Chemical Co. (Ann Arbor, MI, USA). The triglyceride contents were measured in adipose tissue and the results expressed in micromoles of released glycerol per mmol of tissue triglyceride in each reaction.

The rate of fatty acid oxidation was measured by the production of $^{14}\text{CO}_2$ from $[1-^{14}\text{C}]$ palmitic acid using mitochondria fractions from adipose, liver and muscle tissues as described [2]. In brief, mitochondria were isolated from individual tissues as described [3] and mixed with reaction buffer (100 mM sucrose, 10 mM Tris-HCl, 5 mM KH_2PO_4 , 0.2 mM EDTA, 0.3% BSA, 80 mM KCl, 1 mM MgCl_2 , 2 mM L-carnitine, 0.1 mM malate, 0.05 mM coenzyme A, pH 8.0). After adding 2 mM ATP, 1 mM DTT, 0.5 mM palmitic acid and 0.4 $\mu\text{Ci/ml}$ $[1-^{14}\text{C}]$ palmitic acid, the reaction was continued at 37°C for 60 minutes and then stopped with 1 M perchloric acid. The released $^{14}\text{CO}_2$ was captured by filter paper rinsed with concentrated hyamine hydroxide. The filter paper was transferred to scintillation vial for radioactivity counting.

ACC activity. ACC activity was measured as described [4] with modifications. Briefly, tissue was homogenized on ice in buffer containing 50 mM Tris-HCl (pH 7.4), 250 mM mannitol, 1 mM EDTA, 1 mM DTT, 50 mM NaCl, 50 mM NaF, 1 mM PMSF, 5 mM $\text{Na}_2\text{H}_2\text{O}_7$ and protease inhibitor cocktail. After centrifugation at 14,000 g for 30 minutes at 4°C , the supernatant was used as a crude enzyme fraction. The protein concentration was determined by BCA assay (Thermo Scientific, Rockford, IL, USA). For ACC assay, the crude enzyme fraction with equal amount of proteins was incubated with reaction mixture containing 100 mM Tris-HCl (pH 7.5), 1 mM DTT, 2.1 mM ATP, 125 μM acetyl-CoA, 6 mM MgCl_2 , 100 mM KCl, 10 mM sodium citrate, 1mg/ml BSA, 18 mM $\text{NaH}[^{14}\text{C}]\text{O}_3$ (0.5 mCi/mmol) for 30 minutes at 37°C . The reaction was stopped by the addition of 1 M HClO_4 . After centrifugation at 2000 g for 15 minutes, the supernatant was transferred into a vial and dried. The sample was resolved in a scintillation cocktail and the bound $[^{14}\text{C}]$ bicarbonate was quantified by a liquid scintillation counter. ACC activity was expressed in units: 1 unit = 1 nmol fixed $\text{HCO}_3^-/\text{min/mg}$ protein.

ELISA quantification of total biotin. Free biotin and biotinylated proteins in serum and tissue samples were measured using commercially available ELISA kit (Immundiagnosti, Bensheim, Germany) according to manufacturer's instructions. In brief, equal amounts of serum and tissues samples were mixed with HRP-conjugated avidin and incubated for two hours at room temperature. The mixture was then transferred to wells of biotinyl-BSA-coated plate and incubated for another four hours at room temperature. After adding the substrate, the absorbance at 450 nm was measured. The detection range of biotin was 0.15–500 nM.

Synthesis of biotinyl-5'-AMP. Adenylic acid (35 mg, 0.1 mmol, 1 eq.) and d-biotin (25 mg, 0.1 mmol, 1 eq.) were dissolved in 75% aqueous pyridine (0.5 ml) at 0°C. To the solution, DCC (413 mg, 2.0 mmol, 20 eq.) in pyridine (0.5 ml) precooled to 0 °C was added slowly. The mixture was stirred at 0°C for 24 hr. DCC was removed by filtering through a pad of celite. The crude product was purified by preparative HPLC (Gradient: 5-20% CH₃CN/H₂O over 30 min, 20-65% CH₃CN/H₂O over 10 min at a flow rate of 10 ml/min), followed by concentration and lyophilization. The identity and purity of biotinyl-5'-AMP was confirmed by mass spectrometry analysis.

Preparation of stromal vascular cell fraction (SVF) and mature adipocytes. Adipose tissue was digested with collagenase (1 mg/ml) for 30 min at 37°C with shaking. The cell suspensions were filtered through a 40 µm Cell Strainer (BD Biosciences, San Jose, CA, USA) and centrifuged at 500 g for 10 min. The supernatant containing the mature adipocytes was collected. The SVF pellet was washed with lysis buffer (155 mM NH₄Cl, 10 mM KHCO₃, and 0.1 mM Na₂EDTA, pH 7.4) to remove red blood cells. The adipocyte fraction and SVF pellets were subsequently used for Western blotting.

Measurement of tissue NAD⁺/NADH contents. EnzyChrom™ NAD⁺/NADH assay kits (BioAssay Systems, Hayward, CA, USA) were used. In brief, tissues (20 mg) were homogenized in extraction buffers and the total amount of NAD⁺/NADH was measured

according to the instructions from manufacturer. The results were calculated as the amount of NAD⁺ or NADH (nmol) per mg of tissue weight.

Quantitative RT-PCR analysis. Total RNA were isolated from adipose tissue using TRIZOL Reagent (Invitrogen, Carlsbad, CA) and reverse transcribed using Superscript III reverse transcription system (Invitrogen). Oligonucleotide primers were designed using GenScript Online Tools (<http://www.genscript.com/ssl-bin/app/primer>). Primer sequences are listed in Supplementary Table S2. Quantitation of target gene mRNA was performed in 96 well plates using QuantiTect® SYBR®Green PCR Master Mix (Qiagen, Hilden, Germany) and an ABI PRISM 7900 HT Sequence Detection System (Applied Biosystems, Foster city, CA). Quantification was achieved using Ct values that were normalized with beta-actin as a reference control.

Western blotting and co-immunoprecipitation. Antibodies against ACC, acetylated lysine and DYKDDDDK Flag-tag were purchased from Cell Signaling (Beverly, MA, USA). Antibodies against SIRT1 and acetylated histone H4 (K5, K8, K12 and K16) were from Millipore (Billerica, MA, USA). Monoclonal antibody against beta-actin and streptavidin HRP conjugate were purchased from Sigma. For Western Blotting, proteins derived from cell or tissue lysates were separated by SDS-PAGE and transferred to polyvinylidene difluoride membranes. Following blocking, membranes were probed with various primary antibodies to determine different levels of protein expressions. Streptavidin HRP conjugate was used for probing biotinylated proteins. Immunoreactive antibody-antigen complexes were visualized with the enhanced chemiluminescence reagents from GE Healthcare (Uppsala, Sweden).

For co-immunoprecipitation, tissues or cells were solubilized in radioimmunoprecipitation assay lysis buffer. Same amounts of protein lysates (500 µg) were incubated with specific antibody at 4°C overnight on a shaking platform. After washing

extensively with ice-cold PBS, the immunocomplexes were eluted with 0.1 mol/L glycine HCl (pH 3.0) and neutralized for SDS-PAGE and Western blotting.

Cloning and mutagenesis. The BCCP cDNA fragment of human ACC (3420-4457 nt, NM 198839.1) was cloned from HepG2 cells with the primers listed in Supplementary Table S1. After another two rounds of PCR to introduce sequences encoding a myc (EQKLISEEDL) and a Flag (DYKDDDDK) tag at 5' and 3' end, respectively, a NotI/XhoI fragment was subcloned into pcDNA 3.1 (+) vector to produce the mammalian expression vector pcDNA-BCCP.

Molecular docking The ICM-Pro 3.7-2b program [Molsoft] was applied to evaluate the binding of biotin or its metabolites to Sir2 [5]. Hydrogen and missing heavy atoms were added to the structure followed by local minimization using the conjugate gradient algorithm and analytical derivatives in the internal coordinate space. The energetically most favorable tautomeric state of His was chosen. Position of Asn and Gln were optimized to maximize hydrogen bonding. The correct stereochemistry and formal charges were assigned. Biotin was then assigned the MMFF atom types and charges, and subjected to a global energy optimization using the ICM stochastic optimization algorithm. A modified ECEPP/3 force-field with distance-dependent dielectric constant was used for energy calculations as implemented in ICM. The biased probability Monte Carlo minimization method consisted of the following steps: (1) a random conformation change of the free variables according to a predefined continuous probability distribution; (2) local energy minimization of analytical differentiable terms; (3) calculation of the complete energy including non-differentiable terms such as entropy and solvation energy; and (4) acceptance or rejection of the total energy based on the Metropolis criterion and return to step 1. The binding score was evaluated by binding energy, composes of grid energy, continuum electrostatic and entropy terms.

References

- [1] Law IK, Xu A, Lam KS, Berger T, Mak TW, Vanhoutte PM, Liu JT, Sweeney G, Zhou M, Yang B and Wang Y. Lipocalin-2 deficiency attenuates insulin resistance associated with aging and obesity. *Diabetes* 2010; 59: 872-882.
- [2] Hirschey MD, Shimazu T, Goetzman E, Jing E, Schwer B, Lombard DB, Grueter CA, Harris C, Biddinger S, Ilkayeva OR, Stevens RD, Li Y, Saha AK, Ruderman NB, Bain JR, Newgard CB, Farese RV, Jr., Alt FW, Kahn CR and Verdin E. SIRT3 regulates mitochondrial fatty-acid oxidation by reversible enzyme deacetylation. *Nature* 2010; 464: 121-125.
- [3] Zhou M, Xu A, Tam PK, Lam KS, Chan L, Hoo RL, Liu J, Chow KH and Wang Y. Mitochondrial dysfunction contributes to the increased vulnerabilities of adiponectin knockout mice to liver injury. *Hepatology* 2008; 48: 1087-1096.
- [4] Witters LA, Watts TD, Daniels DL and Evans JL. Insulin stimulates the dephosphorylation and activation of acetyl-CoA carboxylase. *Proc Natl Acad Sci U S A* 1988; 85: 5473-5477.
- [5] Chow KH, Sun RW, Lam JB, Li CK, Xu A, Ma DL, Abagyan R, Wang Y and Che CM. A gold(III) porphyrin complex with antitumor properties targets the Wnt/beta-catenin pathway. *Cancer Res* 2010; 70: 329-337.

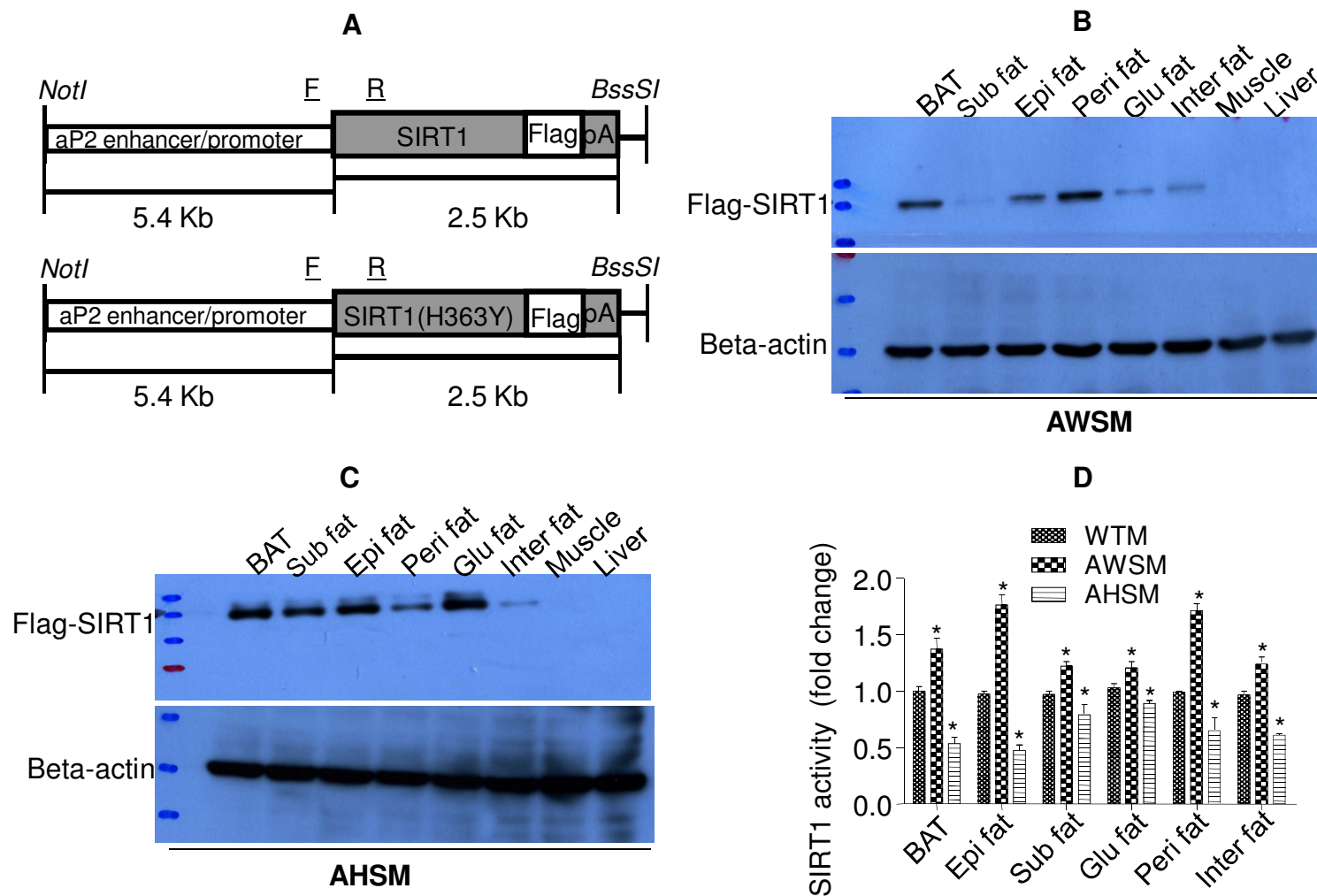
Table S1. List of primers used for cDNA cloning, site-directed mutagenesis and genotyping.

Experiment	Primer sequences
Subcloning hSIRT1	Forward: CTTATCGATATCTCGTCGTGCATCTTTTG Reverse: GGTATCGATGGCTACTTGTTCATCGTCGTCCTTGTAGTCTGATTTGTTTGATGGATAGTT
Mutagenesis for hSIRT1(H363Y)	Forward: TAATT CAGTGT <u>TATG</u> GTTCCTTTGC Reverse: GCAAAGGAAC CATA <u>ACACTG</u> AATTA
Genotyping I (product 483 bp)	Forward: TGGCCCCCATTTGGTCACTCCT Reverse: GCCCGGCCCATTTGTCTCCTT
Genotyping II (product 405 bp)	Forward: GCAAAGGAGCAGATTAGTAGGCGGC Reverse: CGAGGTCGACGGTATCGATGGCT
Genotyping III (PCR-RFLP)	Forward: TGCTCGCCTTGCTGTAGACTTCC Reverse: AAGCGGTTCATCAGCTGGGCA A PCR product 373 bp is digested with <i>NlaIII</i> to generate two fragments of 122 bp and 251 bp in AWSM samples.
Genotyping IV (PCR-RFLP)	Forward: TCCTGGACAATTCCAGCCATCTCT Reverse: AGATGCTGTTGCAAAGGAACCAT A PCR product 160 bp is digested with <i>NlaIII</i> to generate two fragments of 140 bp and 20 bp in AWSM samples.
Subcloning BCCP	Forward_1: GGGCTGAGTGACGGTGGACTGC Reverse_1: AGGGTCCCGGCCACACAAC Forward_2: ACCATGGAACAGAACTGATTAGCGAAGAAGATCTGGGGCTGAGTGACGGTGGACTGC Reverse_2: CTACTTGTTCATCGTCGTCCTTGTAGTCAGGGTCCCGGCCACACAAC Forward_3: AGCACAGTGCGCGCCGCACCATGGAACAGAACTGATTAG Reverse_3: GCCCTCTAGACTCGAGCTACTTGTTCATCGTCGTCCTT

Table S2. List of primers used for quantitative PCR analysis.

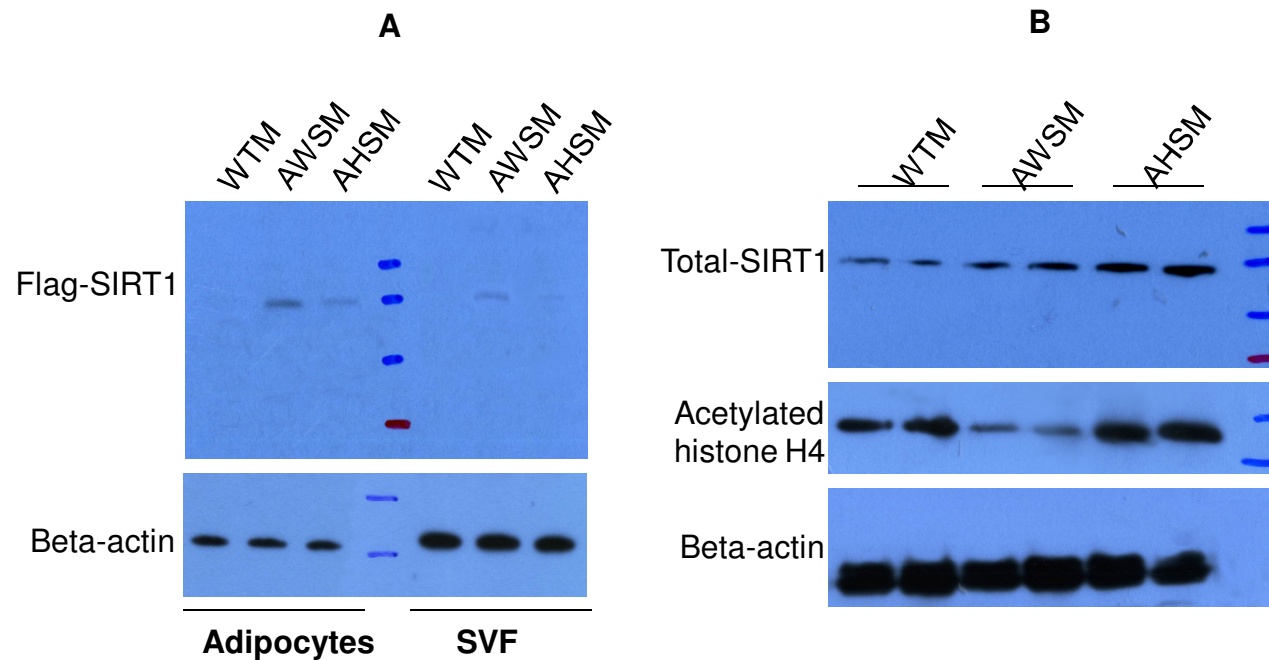
Gene name	Gene symbol	Accession ID	Sequence range	Product size (bp)	Primer sequences
Beta-actin	<i>Actb</i>	gil145966868	930-1107	178	Forward 5'-AGTGTGACGTTGACATCCGT-3' Reverse 5'-CCACCGATCCACACAGAGTA-3'
Adipose triglyceride lipase (ATGL)	<i>Pnpla2</i>	gil254826779	724-868	145	Forward 5'-AACACCAGCATCCAGTTCAA -3' Reverse 5'-GGTTCAGTAGGCCATTCTC -3'
Holocarboxylase (HCS)	<i>Hlcs</i>	gil146149144	1719-1881	163	Forward 5'-TGTGCTCTTCCACTCTGCT-3' Reverse 5'-AAATATCGTTGGGCCACTTC-3'
Biotinidase	<i>Btd</i>	gil270341335	325-469	145	Forward 5'-CAGCCCAGAAGGGTGTGCAGAT-3' Reverse 5'-CGAAAGGGCTCCAGACACGGG-3'
Acetyl-Coenzyme A carboxylase alpha (ACC α)	<i>Acaca</i>	gil125656172	178-339	162	Forward 5'-CCTCCGTCAGCTCAGATACA -3' Reverse 5'-CTGGAGAAGCCACAGTGAAA -3'
Acetyl-Coenzyme A carboxylase beta (ACC β)	<i>Acacb</i>	gil157042797	3696-3892	197	Forward 5'-GGTGGAGTCCATCTTCCTGT -3' Reverse 5'-TGTTTAGCTCGTAGGCGATG -3'
Sodium-dependent vitamin transporter (SVMT)	<i>Slc5a6</i>	gil294979173	1975-2129	155	Forward 5'-CCTGGACTGTTCTTCCCAT-3' Reverse 5'-GGAAGGAGCTGGATCCATTA-3'
Adiponectin	<i>Adipoq</i>	gil87252710	24-293	200	Forward 5'-ACGACACCAAAGGGCTCAGGA-3' Reverse 5'-CCATCACGGCCTGGTGTGCC-3' '
Glucokinase	<i>Gck</i>	gil118129970	48-247	200	Forward 5'-AGA GCA GAT CCT GGC AGA GT -3' Reverse 5'-TGG TTC CTC CCA GGT CTA AG -3'

Supplementary Figure 1



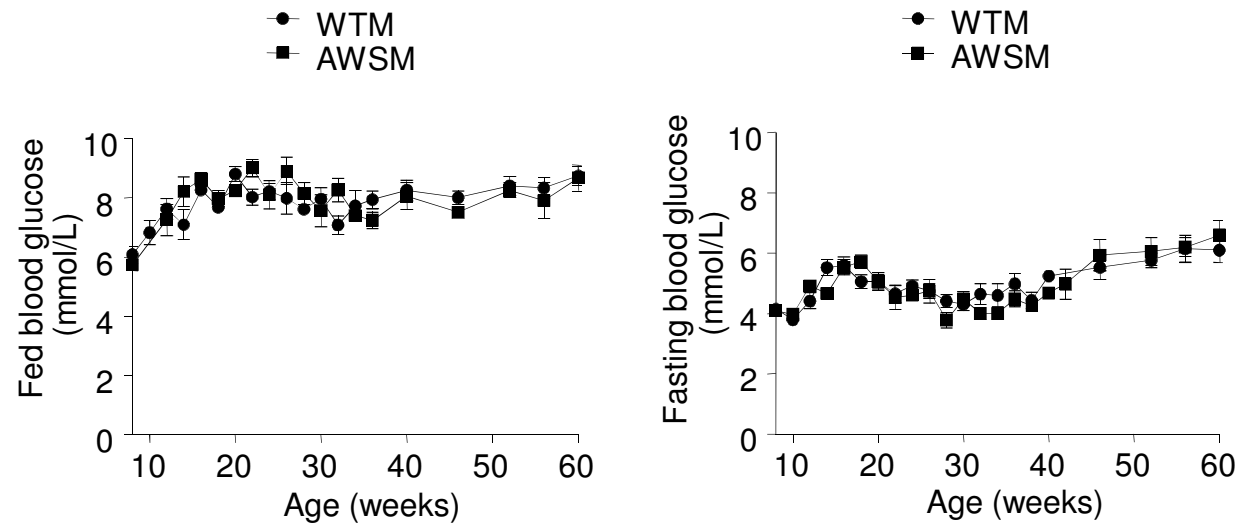
Supplementary Figure 1. Establishment of transgenic mice selectively over-expressing human SIRT1 (hSIRT1) or its mutant hSIRT1(H363Y) in adipose tissues. (A) Fragments of transgenic vectors for overexpressing Flag-tagged hSIRT1 (NM_012238.4) or hSIRT1(H363Y) under the control of an aP2 enhancer/promoter. (B) Representative image of Western blotting analysis of Flag-tagged hSIRT1 expression in tissues collected from AWSM. Beta-actin was probed as loading control. (C) Representative image of Western blotting analysis of Flag-tagged hSIRT1(H363Y) expression in tissues collected from AHSM. Beta-actin was probed as loading control. (D) Adipose SIRT1 activity was measured using commercial assay kits. The results are expressed as fold changes *versus* that of WTM control samples. *, $P < 0.05$ compared with WTM control group (n=3). Epi, epididymal fat; Glu, gluteal fat; Inter, interscapular fat; Peri, perirenal fat; Sub, subcutaneous fat; BAT, brown fat.

Supplementary Figure 2



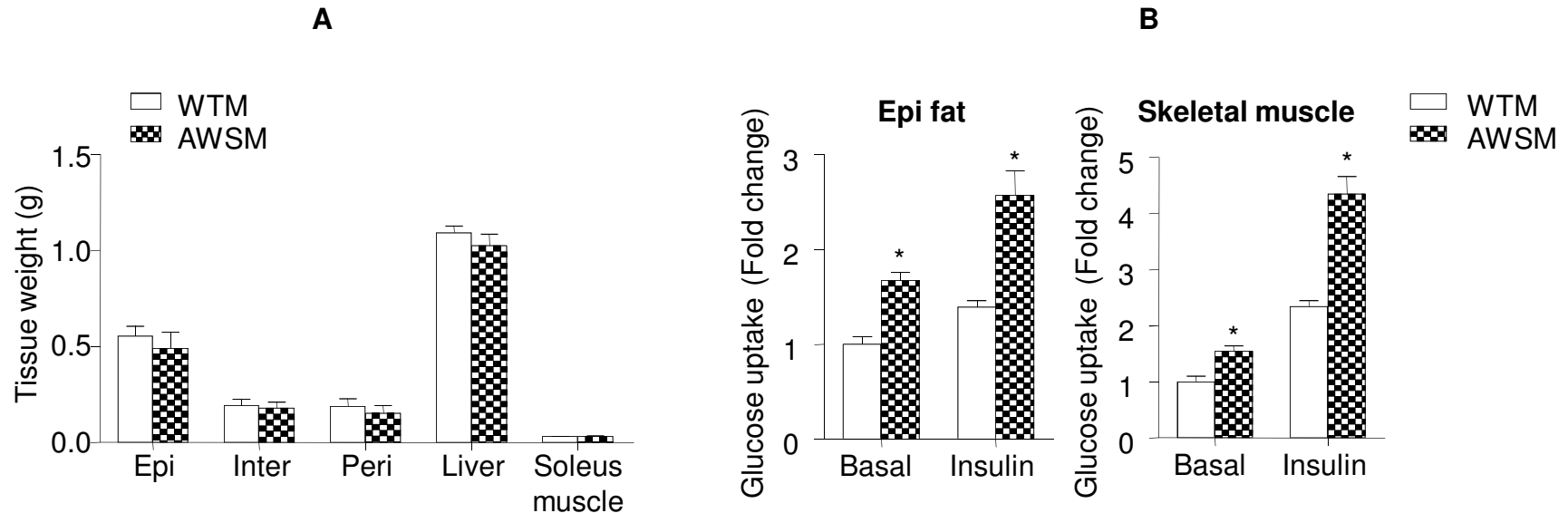
Supplementary Figure 2. Flag-tagged hSIRT1 and hSIRT1(H363Y) could be detected in adipocytes and stromal vascular fractions (SVF) isolated from the fat pads of transgenic animals. (A) Epididymal fat was isolated from WTM, AWSM and AHSM. After digesting with collagenase, adipocytes and SVF pellets were collected as described in Methods. Proteins (50 μ g and 80 μ g for adipocytes and SVF, respectively) were separated by SDS-PAGE and subjected to Western blotting using antibodies against the Flag-tag (top) and beta actin (bottom). (B) Increased expression of SIRT1 protein in adipose tissues of AWSM and AHSM was confirmed by Western blotting using an antibody recognizing both murine and human SIRT1 (top). The amount of acetylated histone H4 (K5, K8, K12, K16) was probed with specific antibody (middle). Beta actin was probed as the loading control (bottom).

Supplementary Figure 3



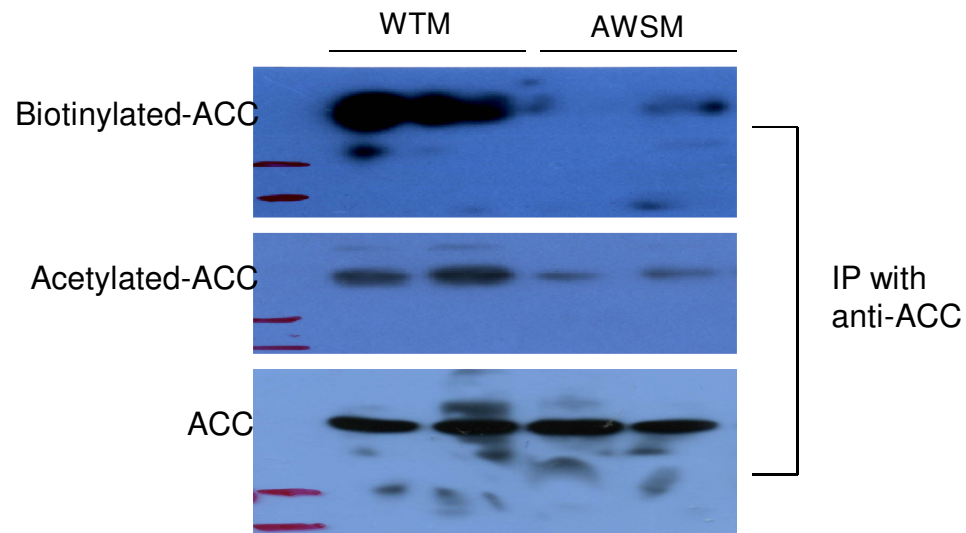
Supplementary Figure 3. Blood glucose levels were not different between WTM and AWSM. Fed blood glucose (left) was measured at 10am in mice fed *ad libitum*. Fasting blood glucose (right) was measured at 10am in mice that were starved for 16 hours.

Supplementary Figure 4



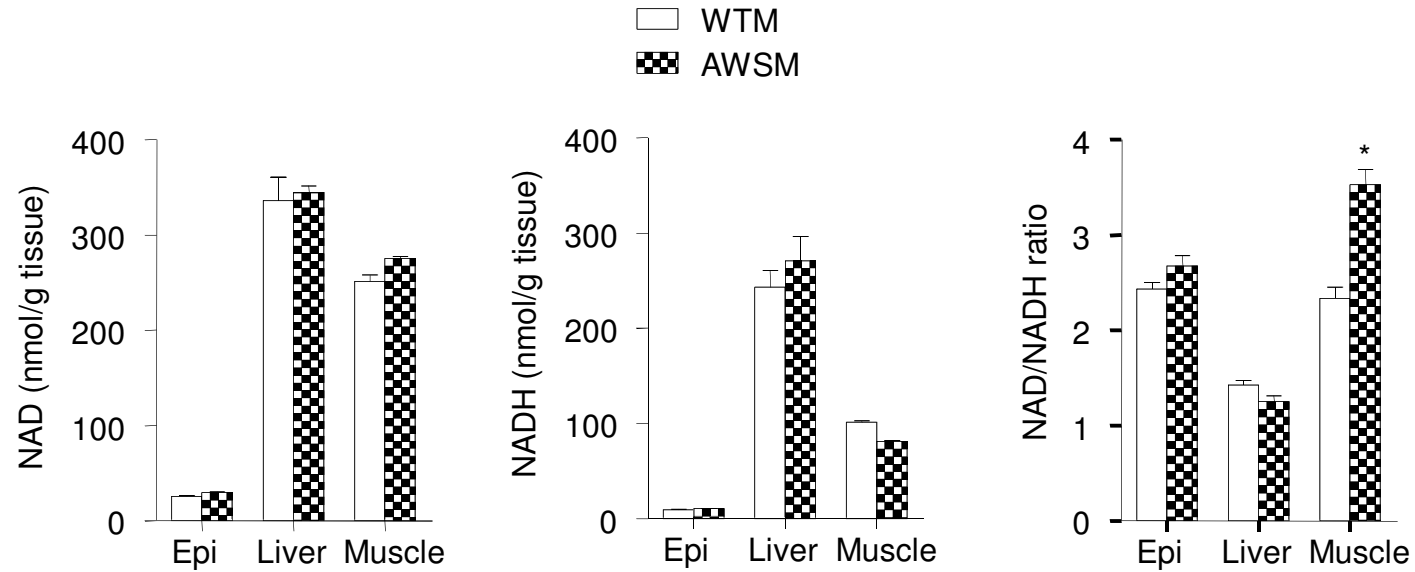
Supplementary Figure 4. Overexpression of hSIRT1 selectively in adipose tissue enhanced peripheral insulin sensitivity. (A) Tissue weights were recorded for WTM and AWSM sacrificed at the age of 36-week old. (B) Basal and insulin-stimulated glucose uptake was evaluated in epididymal (epi) adipose tissue and soleus muscle strips using [^3H]-2-deoxyglucose as a tracer. The results are presented as fold changes against the basal glucose uptake of WTM control group. *, $P < 0.05$ compared with WTM group (n=10).

Supplementary Figure 5



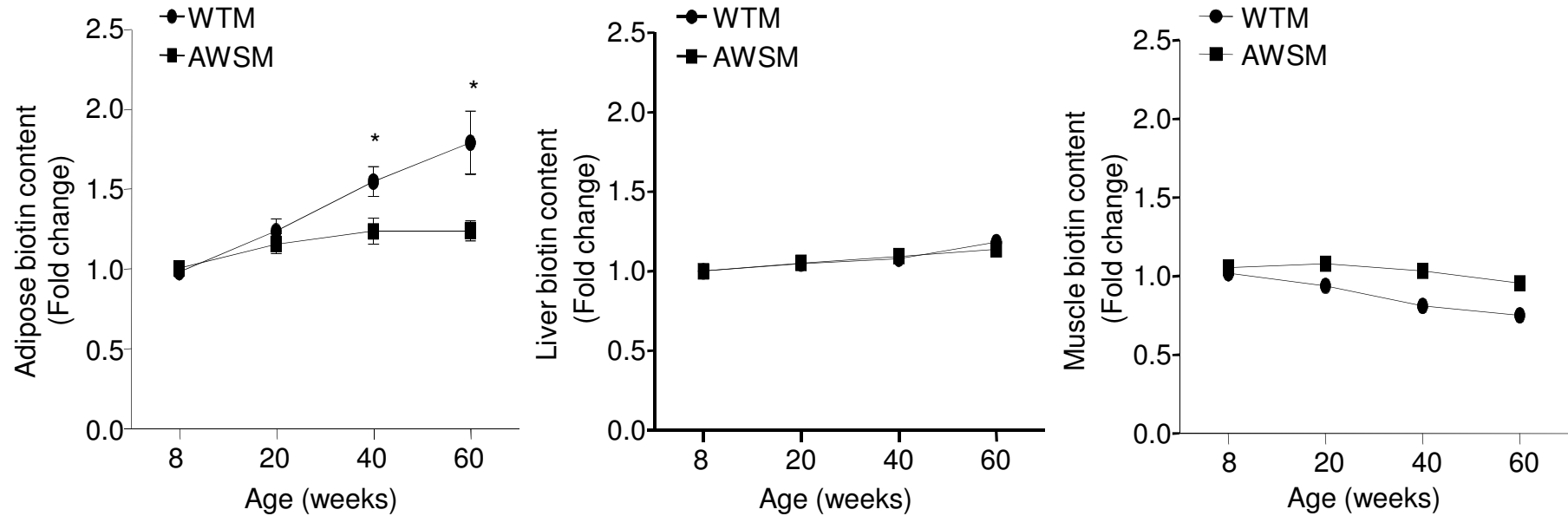
Supplementary Figure 5. Decreased biotinylation and acetylation of ACC in adipose tissues of AWSM. Immunoprecipitation (IP) was performed using specific antibody against ACC. The biotinylation and acetylation levels of the precipitated ACC protein were probed by Western blotting.

Supplementary Figure 6



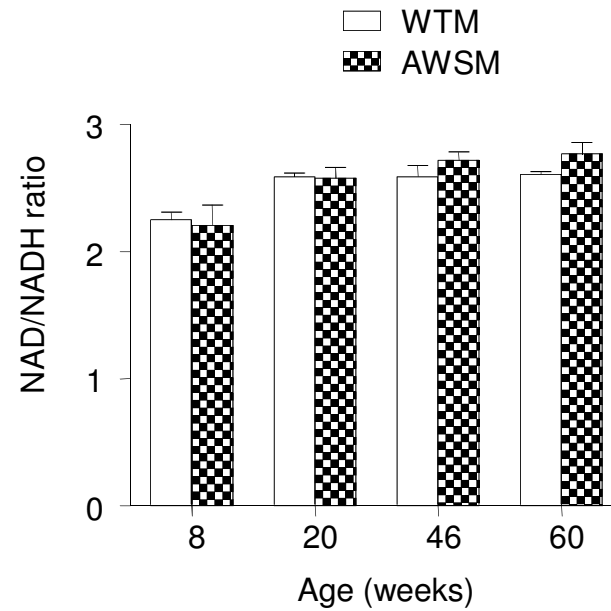
Supplementary Figure 6. Skeletal muscle of AWSM showed significantly increased NAD/NADH ratio. The amount of NAD and NADH was measured in epi fat, liver and skeletal muscle of WTM and AWSM mice (36-weeks old). The ratio of NAD/NADH was calculated and presented in the right panel. *, $P < 0.05$ compared with WTM control group (n=5).

Supplementary Figure 7



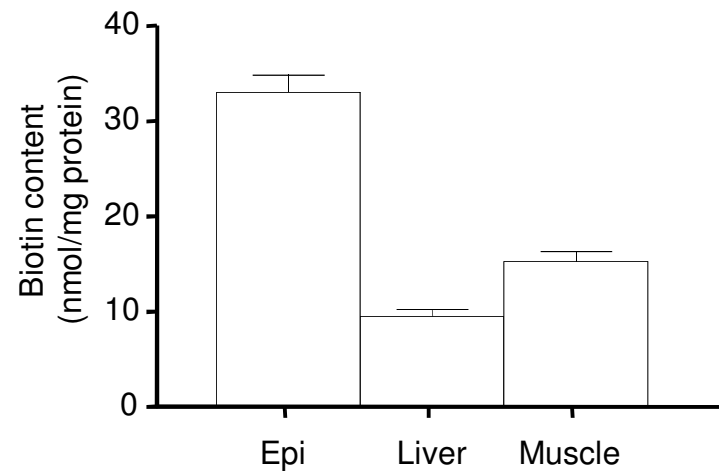
Supplementary Figure 7. Ageing-dependent biotin accumulation in adipose tissue was alleviated in AWSM. Tissue extracts from epididymal fat, liver and skeletal muscle of WTM and AWSM were used for measuring total biotin content using the commercially available ELISA kits as described in Methods. The results are presented as fold change against the values of 8-weeks old mice. *, $P < 0.05$ compared with WTM control group (n=3-6).

Supplementary Figure 8



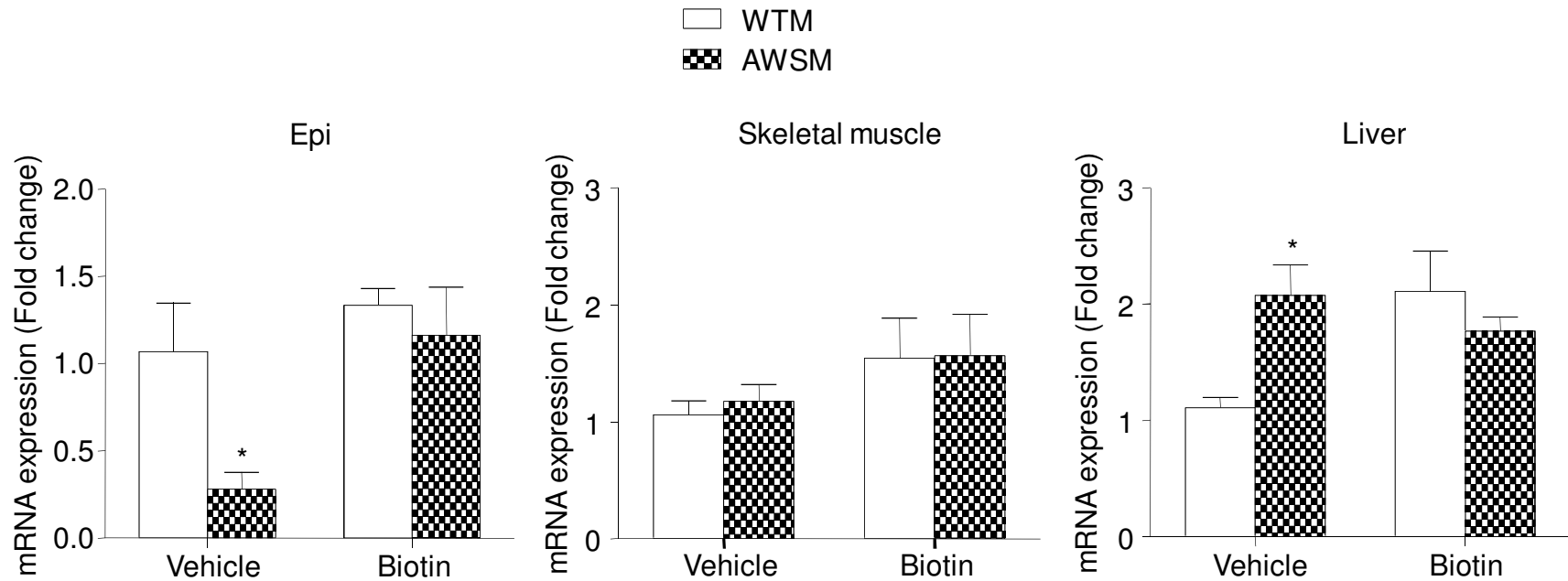
Supplementary Figure 8. The NAD/NADH ratio in adipose tissues of WTM and AWSM was similar. The amount of NAD and NADH was measured in epididymal fat collected from WTM and AWSM at different ages. The ratio of NAD/NADH was calculated and presented. (n=5)

Supplementary Figure 9



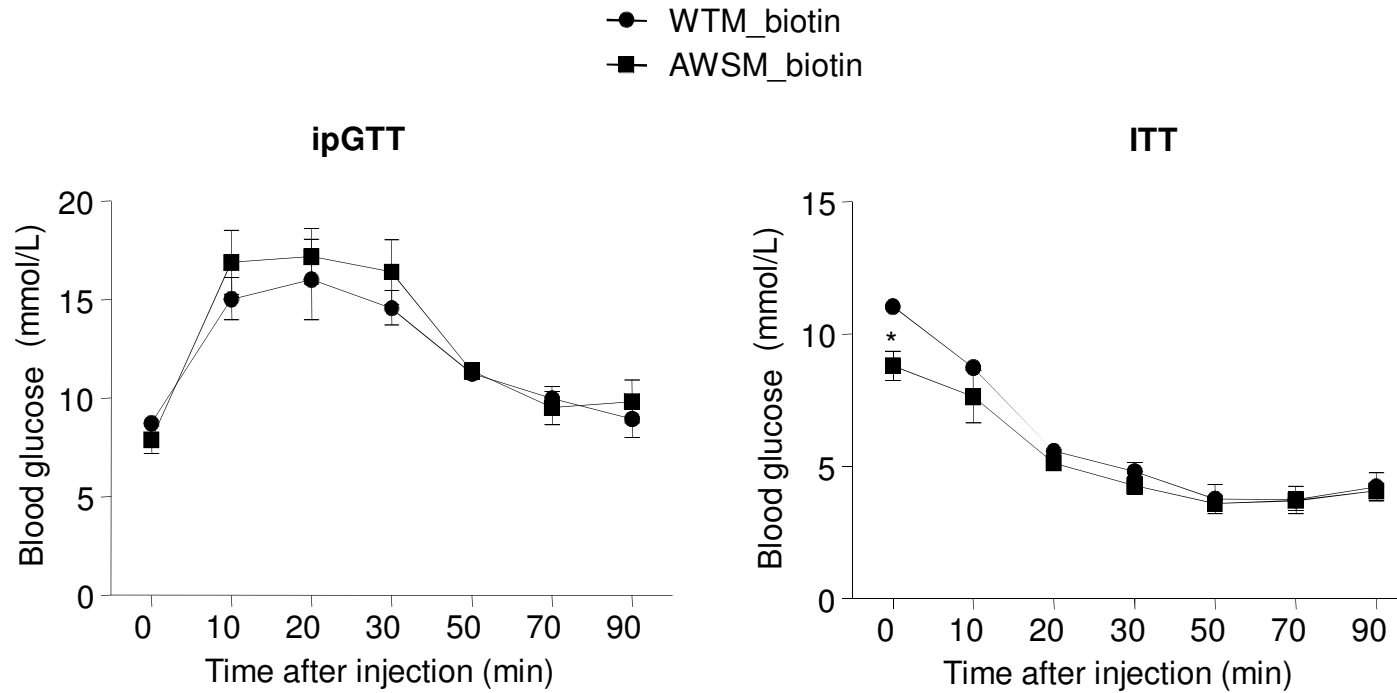
Supplementary Figure 9. Biotin contents in epididymal tissue (epi), liver and skeletal muscle of wild type C57BL/6J mice. The amount of biotin was measured using commercial kit and results calculated against protein content. (n=5)

Supplementary Figure 10



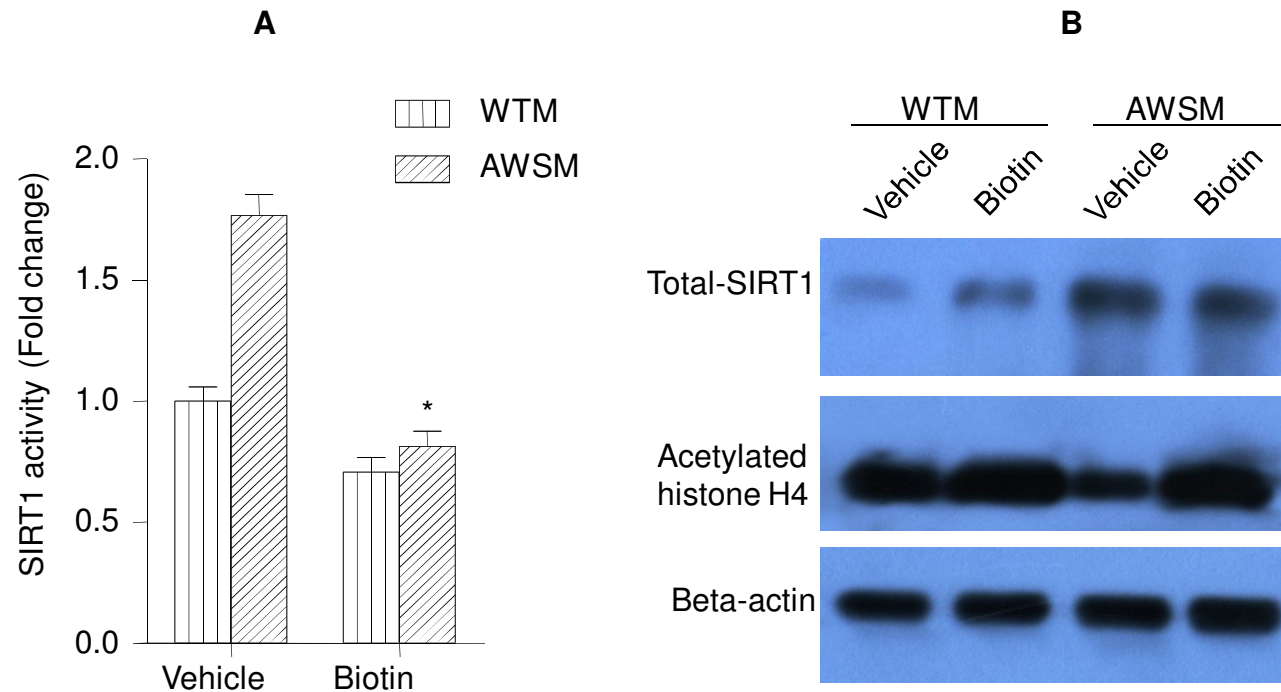
Supplementary Figure 10. Chronic supplementation of biotin abolished the differences of glucokinase gene expression between WTM and AWSM mice. Epididymal adipose (epi), skeletal muscle and liver tissues were collected from vehicle- or biotin-treated WTM and AWSM mice for quantitative PCR analysis of glucokinase mRNA levels. *, $P < 0.05$ compared with corresponding WTM control group (n=3-5).

Supplementary Figure 11



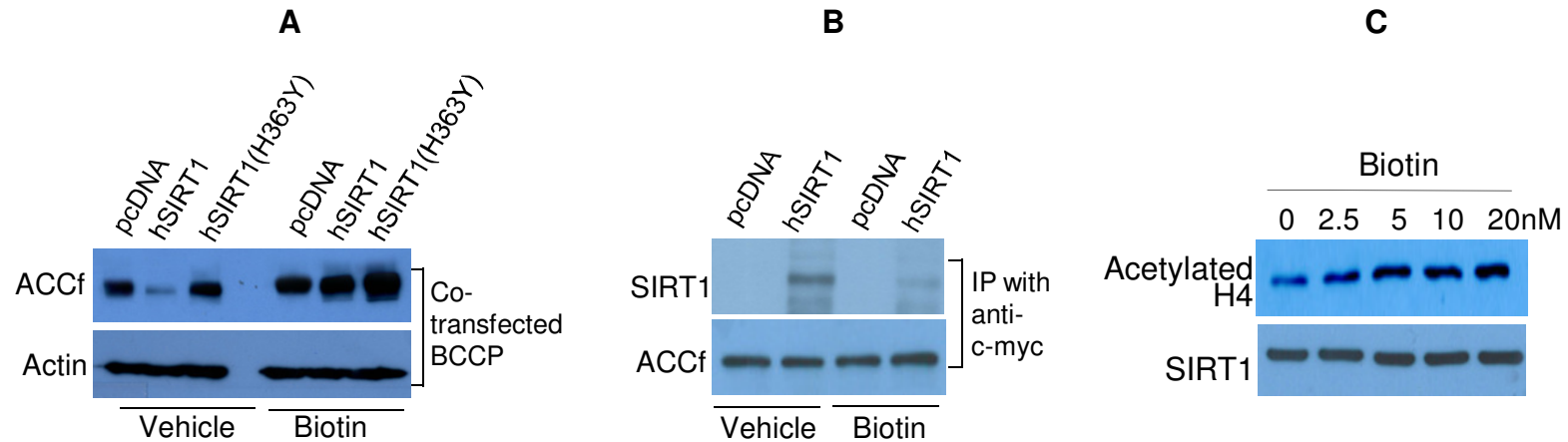
Supplementary Figure 11. Chronic supplementation of biotin abolished the beneficial metabolic effects of adipose SIRT1 in AWSM. Intraperitoneal glucose tolerance tests (ipGTT) and insulin tolerance tests (ITT) were performed for WTM and AWSM (60-weeks old) subjected to biotin treatment. Biotin-treated WTM showed significantly higher blood glucose levels after six hours of fasting. *, $P < 0.05$ compared with biotin-treated WTM group (n=10).

Supplementary Figure 12



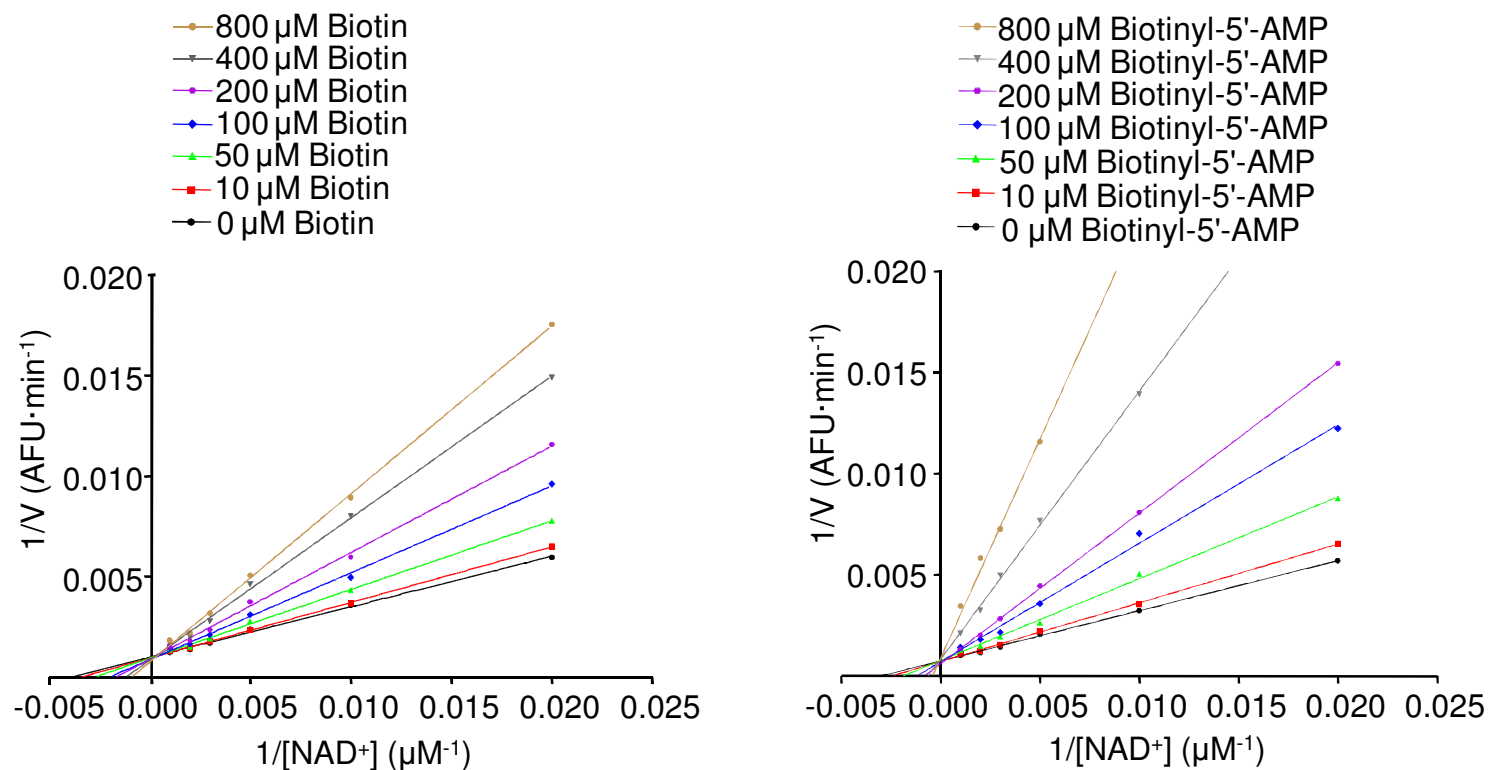
Supplementary Figure 12. Biotin supplementation reduced adipose SIRT1 activity. Epididymal fat was isolated from WTM and AWSM treated with vehicle or biotin. **(A)** SIRT1 activity was measured in tissue lysates using commercial assay kits as described in Methods. **(B)** Proteins (100 μ g) were separated by SDS-PAGE and subjected to Western blotting using antibodies against SIRT1 (human and murine) and acetylated histone H4 (K5, K8, K12, K16). Beta actin was probed as loading control. *, $P < 0.01$ compared with vehicle-treated AWSM (n=6)

Supplementary Figure 13



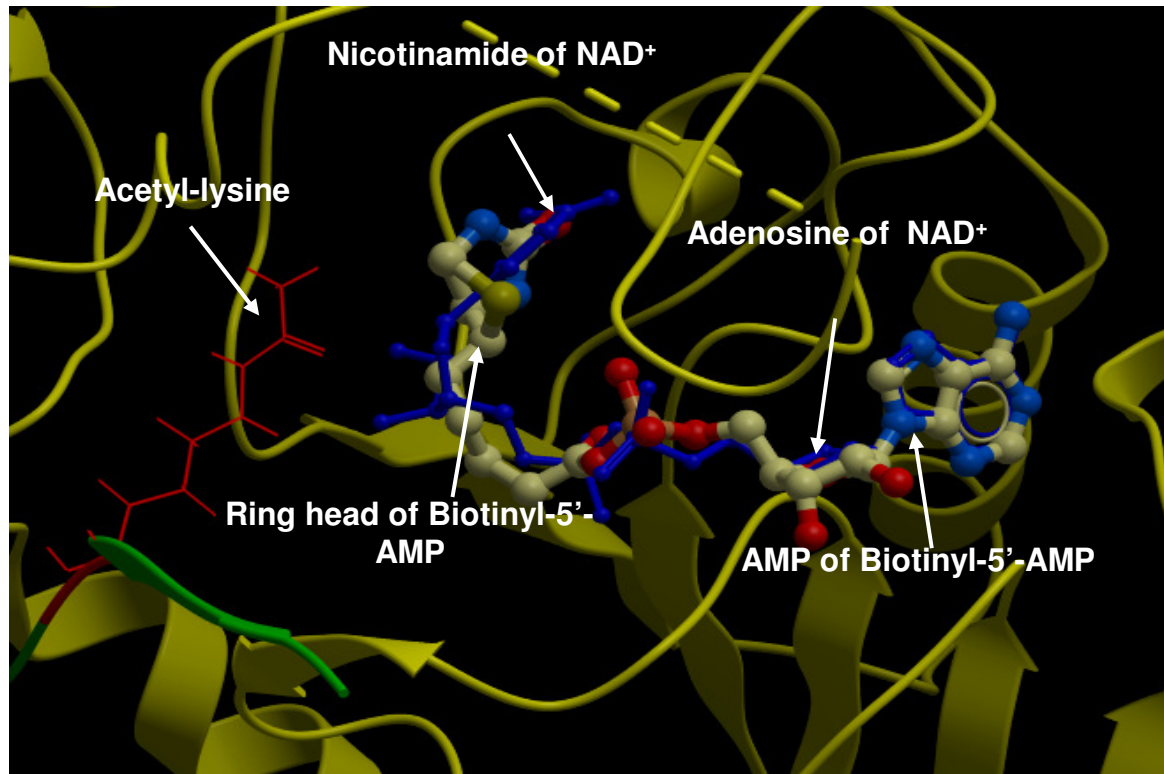
Supplementary Figure 13. Biotin inhibited SIRT1-mediated regulation of ACC protein expression. (A) The protein abundance of ACCf was evaluated in 3T3-L1 cells co-transfected pcDNA-BCCP, together with pcDNA, pcDNA-hSIRT1 or pcDNA-hSIRT1(H363Y). Cells were treated with vehicle or biotin (10 nM). Anti-Flag antibody was used for detecting ACCf by Western blotting. (B) Immunoprecipitation was performed in 3T3-L1 cells overexpressing hSIRT1 and/or ACCf, using antibodies against c-myc tag. The presence of SIRT1 in the immuno-complex was probed with specific antibodies recognizing both murine and human SIRT1. (C) Acetylated histone H4 was detected by Western blotting in 3T3-L1 adipocytes treated with increasing concentrations of biotin.

Supplementary Figure 14



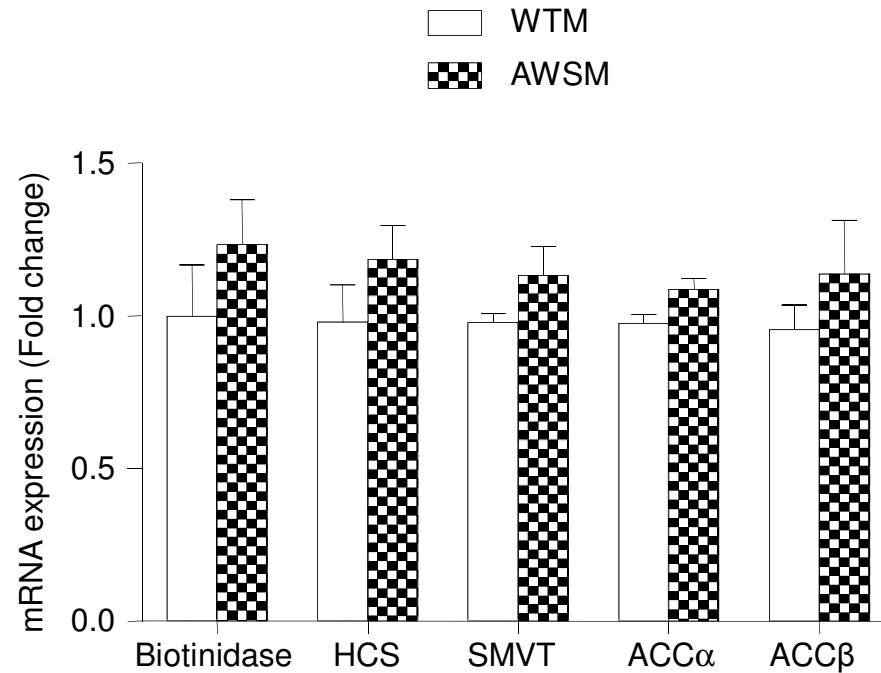
Supplementary Figure 14. Biotin and biotinyl-5'-AMP acted as competitive inhibitors of SIRT1. **Left:** SIRT1 activity was measured in the presence of different concentrations of NAD⁺ and/or biotin. **Right:** SIRT1 activity was measured in the presence of different concentrations of NAD⁺ and/or biotinyl-5'-AMP. Data are shown as Lineweaver-Burk double-reciprocal plots of arbitrary fluorescence units (AFU) min⁻¹ versus $1/[NAD^+]$ (μM⁻¹).

Supplementary Figure 15



Supplementary Figure 15. Docking model (lowest-energy) for the binding of biotinyl-5'-AMP with Sir2 homologue (ribbon form, yellow). Biotinyl-5'-AMP (thick ball and stick format, blue for N, red for O, and white for C) occupies the binding pocket of NAD⁺ (thin ball and stick format, blue). Green ribbon represents the p53 peptide (the acetyl-lysine residue is shown in red wire format).

Supplementary Figure 16



Supplementary Figure 16. The mRNA expression levels of biotinidase, holocarboxylase synthetase (HCS), sodium-dependent multivitamin transporter (SMVT), acetyl CoA carboxylase alpha (ACC α) and ACC β in adipose tissues of AWSM were not significantly different from those of WTM. RNA was extracted from epididymal fat of WTM and AWSM. Quantitative PCR was performed for comparing the mRNA expression levels of the above genes. (n=5)